Multi-omics analysis in human retina uncovers ultraconserved *cis*-regulatory elements at rare eye disease loci

Victor Lopez Soriano[*1,2], Alfredo Dueñas Rey[*1,2], Rajarshi Mukherjee[3], Genomics England Research Consortium[4], Frauke Coppieters[1,2,5], Miriam Bauwens[1,2], Andy Willaert[1,2], Elfride De Baere[1,2]

1- Department of Biomolecular Medicine, Ghent University, Ghent, Belgium.
2- Center for Medical Genetics, Ghent University Hospital, Ghent, Belgium.
3- Department of Ophthalmology, St James's University Hospital, Leeds, UK.
4- Genomics England, London, UK.
5- Department of Pharmaceutics, Ghent University, Ghent, Belgium.

*equal contribution

Corresponding author: Elfride De Baere (elfride.debaere@ugent.be)

ABSTRACT

Cross-species genome comparisons have revealed a substantial number of ultraconserved non-coding elements (UCNEs). Several of these elements have proved to be essential tissue- and cell type-specific *cis*-regulators of developmental gene expression. Here, we characterized a set of UCNEs as candidate CREs (cCREs) during retinal development and evaluated the contribution of their genomic variation to rare eye diseases, for which pathogenic non-coding variants are emerging. Integration of bulk and single-cell retinal multi-omics data revealed 594 genes under potential *cis*-regulatory control of UCNEs, of which 45 are implicated in rare eye disease. Mining of candidate *cis*-regulatory UCNEs in WGS data derived from the rare eye disease cohort of Genomics England revealed 178 ultrarare variants within 84 UCNEs associated with 29 disease genes. Overall, we provide a comprehensive annotation of ultraconserved non-coding regions acting as cCREs during retinal development which can be targets of non-coding variation underlying rare eye diseases.

KEYWORDS

Ultraconserved non-coding elements (UCNEs), retina, single-cell, multi-omics, enhancer, *cis*-regulatory elements (CREs), genomic variation, rare eye disease.

INTRODUCTION

The 'dark matter of the genome' harbors functional *cis*-regulatory elements (CREs) such as promoters, enhancers, silencers, and insulators, whose orchestrated activity is essential to provide spatial and temporal patterns of gene expression that ensure proper tissue development and homeostasis (Field & Adelman, 2020; Spielmann & Mundlos, 2016). The influence of these regulatory elements on their target genes spans within architectural chromatin units known as topologically associating domains (TADs), demarcated by boundaries enriched in CTCF and cohesin proteins (Dixon et al., 2012). Due to their high context specificity, the annotation of candidate CREs (cCREs) poses an attractive yet challenging task. In this regard, the Encyclopedia of DNA Elements (ENCODE) (Abascal et al., 2020; Dunham et al., 2012) represents a powerful tool to characterize functional cCREs, as it provides a robust inventory of well-defined cCREs supported by epigenetic data derived from a wide variety of both human tissues and cell types.

Over the past decades, comparative genomics have been made progress to map functional cCREs by establishing cross-comparison between species. As a result, several databases of non-coding sequences that exhibit extremely high conservation have been generated, including UCEs (Bejerano et al., 2004; Lomonaco et al., 2014), UCNEs (Dimitrieva & Bucher, 2013), ANCORA (Engström et al., 2008) and CONDOR (Woolfe et al., 2007). A direct comparison of these resources is, however, not straightforward due to the intrinsic differences in the scopes of these databases. One of the most comprehensive resources is UCNEbase, which comprises exclusively >200bp-long non-coding genomic regions that exhibit ≥95% sequence identity between human and chicken. The selection of these two species was based on both biological and technical arguments, namely their considerable evolutionary distance enhancing the accuracy in identifying functional elements, and the high-quality of their respective genome assemblies. In total, 4,351 regions across the genome comply with the criteria and are listed as ultraconserved non-coding elements (UCNEs) (Dimitrieva & Bucher, 2013). The vast majority of these highly constrained elements cluster around key developmental genes, such as *PAX6*,

and have been long hypothesized to act as tissue-specific transcriptional regulators (Dimitrieva & Bucher, 2013; Polychronopoulos et al., 2017). Ultraconserved CREs have been shown to be consistently depleted of common variants (Drake et al., 2006; Snetkova, Ypsilanti, et al., 2021), indicating that purifying selection has shifted ultraconserved CRE-derived allele frequencies towards magnitudes similar to those observed for missense variants (Drake et al., 2006), hence reinforcing that variation within these regions is more likely to have functional consequences.

Due to the wide implementation of whole genome sequencing (WGS) in human genetic studies and ambitious initiatives such as the 100,000 Genome Project (100kGP) launched by Genomics England (GEL) (Smedley et al., 2021), previously overlooked regions within the vast non-coding fraction of the genome have been investigated in patients with rare diseases and have shown an emerging role of non-coding variants in disease pathogenesis. Two remarkable examples of functional evidence of disease driven by disruption of conserved CREs can be found precisely in the rare eye disease field, in which mutations located within highly conserved non-coding regions have been linked to developmental defects. A first example is a *de novo* single nucleotide variant (SNV) in an ultraconserved enhancer (SIMO element) 150 kb downstream of an intact *PAX6* transcriptional unit, found in a case with aniridia (Bhatia et al., 2013). Second, tandem duplications within a gene desert downstream the *IRXA* cluster (Cipriani et al., 2017; Small et al., 2016) have been found in patients affected by North Carolina Macular Dystrophy (NCMD); the shared duplicated region harbors an enhancer element defined as UCNE that could act as a *cis*-regulator during retinal development (Van de Sompele et al., 2022).

The retina is a heterogeneous tissue composed of neuronal (rod and cone photoreceptors, bipolar cells, ganglion cells, horizontal cells, and amacrine cells) and non-neuronal cell types (astrocytes, Müller cells and resident microglia) that arise from the common pool of retinal progenitor cells (RPCs) (Turner et al., 1990; Turner & Cepko, 1988). This cellular complexity is the result of spatiotemporally controlled gene expression programs during retinal development, requiring concerted action of thousands of CREs (Lyu et al., 2021; X. Zhang et al., 2023). In the wide spectrum of retinopathies,

inherited retinal diseases (IRDs) represent a leading cause of early-onset vision impairment affecting over 2 million people worldwide. Despite targeted panel-based sequencing and whole exome sequencing (WES)-based genetic testing 30-50% of IRD cases remain unsolved (Ellingford et al., 2016; Haer-Wigman et al., 2017), raising the hypothesis that disease-causing mutations are found in the non-coding genome that are mostly not covered by standard genetic testing.

In this study we set out to annotate UCNEs as cCREs that modulate gene expression during retinal development (Fig. 1A) and that can play a role in retinopathies such as IRDs. Firstly, we performed a comprehensive integration of publicly available multi-omics datasets derived from human retina based on biochemical features associated with regulation of gene expression. Secondly, UCNEs co-localizing with genomic regions showing regulatory activity were linked to target genes that exhibit expression in the retina. Finally, we evaluated the contribution of genomic variation within these regions to rare eye diseases. This allowed us to identify an ultrarare SNV in a candidate *cis*-regulatory UCNE located upstream *PAX6* in a family displaying autosomal dominant foveal abnormalities, for which we provide functional evidence based on transgenic enhancer assays in zebrafish. Overall, this work has improved the functional annotation of UCNEs in human retina representing understudied targets of non-coding variation that may explain missing heritability in rare eye diseases.

RESULTS

Integration of bulk and single-cell multi-omics data enables the identification of 1,487 UCNEs with a candidate *cis*-regulatory role in human retina

The wealth of publicly available data allowed the integration of transcriptomic (bulk and scRNA-seq) and epigenomic (DNase-seq, scATAC-seq, ChIP-seq) data to evaluate the regulatory capacity of UCNEs over the major developmental stages of human retina. More specifically, to identify which UCNEs might have a potential *cis*-regulatory role, an intersection was performed with genomic regions characterized by an open chromatin context in the retina at different developmental stages, as supported either by DNase (ENCODE) or scATAC-seq (Thomas et al., 2022) peaks. This resulted in a

total of 1,487 UCNEs, i.e., approximately one third of UCNEs display a retinal open context (Fig. 1B, Supplementary Table 1) (hereinafter referred to as putatively active UCNEs). Approximately 80% of the DNase-seq peaks were also supported by scATAC-seq, hence defining high-confidence candidate *cis*-regulatory UCNEs (Fig. 1B). Nevertheless, to account for differences in time points between datasets, all 1,487 UCNEs were included in downstream analyses. Apart from the display of a retinal open chromatin context, we also evaluated the overlap between UCNEs and genomic regions featured by markers associated with regulation of gene expression. A total of 834 UCNEs were found to display at least one of the assessed features in the interrogated retinal developmental stages; more specifically 111 UCNEs were identified to display the active enhancer mark H3K27ac, of which most (95%) also exhibit other histone marks related to active enhancers (H3K4me1 and H3K4me2) (Fig. 1B). Out of these 111 UCNEs, 33 were found to maintain signatures consistent with enhancer activity (H3K27Ac) at adult stage. Table 1 and Supplementary Tables 1,2 include summarized and detailed overviews of the number of identified UCNEs per marker and stage, respectively.

Table 1. Overview of the number of events based on the peak identification for each marker at the different stages of retinal differentiation. Abbreviations: FW: fetal weeks.

	Stage				
ChIP-seq	**FW13/14**	**FW15/16**	**FW18/20**	**FW23/24**	**Total Unique**
H3K27ac	73	45	74	94	127
H3K4me1	235	490	48	323	582
H3K4me2	347	354	256	225	465
H3K4me3	94	124	102	97	136
H3K27me3	119	54	128	126	154
H3K9/14Ac	51	76	36	31	94
H3K9me3	0	1	1	29	29
Pol II	17	66	59	55	106
CTCF	51	69	22	37	71

To investigate the functional relevance of the putative regulatory UCNEs, we performed a correlation with the 1,942 experimentally validated human non-coding fragments of the VISTA Enhancer Browser (Fig. 1C). Out of these 1,942 elements, approximately 50% (998/1,942) display enhancer activity. When overlapped with all 4,135 UCNEs, a slight increase of positive elements (505/922) is observed;

however, when only the identified retinal accessible UCNEs were considered, roughly 68% were found to be positive (272/402), thereby reinforcing their predicted regulatory role (Fig. 1C). Interestingly, evaluation of the anatomical description of the reporter gene expression patterns of these 272 elements revealed a potential enrichment in eye (Fig. 1D). An illustrative example of one of these elements and its corresponding multi-omics-based characterization is shown in Fig. 1E-F.

In silico **prediction and integration of retinal chromatin conformation data identify putative target genes under UCNE *cis*-regulation**

We made use of the *GREAT* algorithm to assign potential target genes to the identified putatively active UCNEs and thus assess their association with genes expressed in the retina (Granja et al., 2021). A total of 724 target genes were assigned to the initially identified 1,487 UCNEs displaying candidate *cis*-regulatory activity. The vast majority (74.5%) of queried regions were assigned as putatively regulating two genes based on the used association rule (Fig. 2A). Furthermore, most of these regions were found to be located at 50-500kb from the TSS of the regulated target genes regardless of their orientation (Fig. 2B). Out of these 724 target genes, 594 (81.9%) are expressed in the retina in at least one of the interrogated developmental stages (52 to 136 days post-conception). To evaluate further whether chromatin contacts between the UCNEs and the promoters of their target genes can occur in retina, we integrated the 2,948 retinal TADs identified by Marchal et al. (Marchal et al., 2022). A large majority (393/594) of the target genes were found to be in TADs also harboring their associated UCNE (Supplementary Table 1). These genes were then used as input for Gene Ontology analysis, which revealed an overrepresentation of terms related to regulation of transcription and differentiation, thereby confirming the expected roles of UCNEs as tissue-specific CREs during development, particularly of the nervous system (Fig. 2C; Supplementary Table 3).

As a last layer of characterization of these putatively active UCNEs and their candidate target genes, we assigned to each target gene cell-type specificity information based on expression data. Out of the 1,487 putatively active UCNEs, 808 (54.3%) displayed a cell-type specific open chromatin context

158 consistent with their target gene(s) expression signature(s) (Supplementary Table 1). Furthermore, we
159 evaluated the overlap between the sets of target genes assigned to UCNEs by *GREAT* followed by gene
160 expression filtering and those mapped by implementing the peak-to-gene linkage method on the
161 scATAC-seq data. Although a substantial number of target genes overlapped between both methods
162 (Supplementary Table 4), it is noteworthy to mention that almost half of the UCNEs were assigned to
163 different target genes, most likely due to differences in the annotations employed by both methods.

164 **Mining of WGS data from a rare eye disease cohort reveals rare variants within putatively**
165 **active UCNEs**

166 Out of the 594 putative target genes under UCNE *cis*-regulation, 45 were found to be previously linked
167 to a rare eye disease phenotype, of which 23 are IRD genes and 19 are also associated with other
168 developmental disorder phenotypes (Supplementary Table 5). Considering the extreme selective
169 constraints of UCNEs, we hypothesized that genetic changes in these regions could contribute to
170 disease. Therefore, we evaluated the genomic variation within the putatively active UCNEs associated
171 with these 45 disease genes in a sub-cohort of individuals affected by rare eye diseases (n = 3,220,
172 Supplementary Table 6) from the 100,000 Genomes Project (Fig. 3A).

173 As expected, a depletion of common variation (MAF>1%) was observed across these regions (Fig. 3B).
174 This depletion was found to be not only restricted to the examined sub-cohort but rather constitutes
175 a more general phenomenon. In particular, UCNEs were found to exhibit significantly lower genome-
176 wide residual variation intolerance score (gwRVIS) (Vitsios et al., 2021) values compared to a set of
177 randomly selected genomic regions, thereby reflecting their high intolerance to genomic variation (Fig.
178 3C).

179 A total of 431 (426 SNVs and 5 SVs) ultrarare variants, i.e., absent from reference population public
180 databases, were identified in 199 putatively active UCNEs linked to these 45 genes (Supplementary
181 Table 7). Additionally, we computed the allele frequency distribution of all variants retrieved within a
182 selection of 25 of these disease genes and compared it against that of their corresponding UCNE. As

before, a distinct depletion of common variation was observed, thereby further supporting the specificity of the overlap of (ultra-)rare variants and UCNEs (Fig. S2).

Notably, out of the 5 identified SVs, one corresponds to the known shared duplicated region downstream of *IRX1*, located within the NCMD-linked *MCDR3* locus [MIM: 608850]; in particular, this duplication, identified in 8 affected individuals of 4 different families segregating macular defects consistent with NCMD, involves a UCNE (*IRXA_Aladdin*) exhibiting chromatin accessibility in developing horizontal cells. Finally, out of these ultrarare variants, 178 are located within 84 UCNEs displaying histone modification marks (in at least one of the interrogated stages), associated with 29 genes. This set defined our primary search space for variants with potential functional effects and further assessment.

An ultrarare SNV in an active UCNE upstream of *PAX6* found in a family segregating autosomal dominant foveal anomalies

We identified an ultrarare SNV (chr11:31968001T>C) within a candidate *cis*-regulatory UCNE located ~150kb upstream of *PAX6* (*PAX6_Veronica*). This variant was found in four individuals of a family segregating autosomal dominant foveal abnormalities (Fig. S3A-B; Supplementary Table 8). A *CFH* missense variant (c.1187A>G, p.Asn396Ser) was initially reported in the affected individuals but could not explain the foveal anomaly. Given the phenotype, a variant screening was performed with a particular focus on the *PRDM13* and *IRX1* NCMD loci, both associated with foveal or macular mis-development. A total of three and two SNVs within the *IRX1* and *PRDM13* loci respectively were found to segregate with disease. However, these SNVs are present in individuals from reference population databases and are not located in genomic regions displaying *cis*-regulatory features (Supplementary Table 9). Equally, loci associated with foveal hypoplasia, nystagmus and hypopigmentation (*AHR*, *FRMD7*, *GPR143*, and *SLC38A8*) were assessed for SNV or SV segregating with disease. No other (likely) pathogenic variants in these loci or any other known IRD/rare eye disease gene were identified in the affected cases (Supplementary Table 9).

The identified chr11:31968001T>C variant affects a nucleotide residue that is conserved for at least 360 million years of evolution that separate humans from *X. tropicalis*. *In silico* assessment of this variant and flanking sequence pointed to a likely deleterious effect and revealed a predicted disruption of several TF binding motifs (Supplementary Table 9). More specifically, this variant is located within a UCNE (*PAX6_Veronica*) that is catalogued as a cCRE in ENCODE (EH38E1530321), featured by distal enhancer-like signatures in bipolar neurons. Regarding its retinal context, this UCNE displays accessible chromatin in the early stages of retinal development (7/8 gestational weeks), and in particular in ganglion cell precursors (Fig. 4A-B). Importantly *PAX6* is expressed within this pool of cells and, interestingly, this expression appears to be enriched within a specific sub-population, as observed from the distribution of expression values across all the cells composing this cluster (Fig. S4). Additionally, this UCNE was found to display the active enhancer mark H3K4Me1 at the earliest time points available for this dataset (13/14 and 15/16 gestational weeks).

This region has also been functionally validated in transgenic mouse assays (VISTA element hs855), which revealed gene enhancer activity mainly in the forebrain and, to some extent, in the retina (3/6 embryos) (Fig. 5A). A closer assessment of this UCNE with regard to its proximity to the *PAX6* promoter in other species revealed its syntenic conservation up to zebrafish; interestingly, this element localized in closer proximity to the *PAX6* promoter in species like *X. tropicalis* (60kb distance from the TSS) or *Danio rerio* (15kb distance from the *pax6a* TSS) (Fig. S5).

In vivo **enhancer assays in zebrafish support the association between candidate *cis*-regulatory UCNE and *PAX6***

Given the putative retinal activity suggested by the VISTA enhancer assay for this UCNE, we performed zebrafish enhancer assays to gain further insights into its regulatory range of action. We found consistent reporter expression in several regions, including the forebrain, hypothalamus/otic vesicle, somites, nosepit and eye. Importantly, we observed that the GFP expression in the eye initiated in a small fraction of the embryos at 2 dpf (4/22 GFP^+ embryos) increasing to a larger proportion of the

233 embryos by3 dpf (21/22 GFP^+ embryos) and eventually disappeared from 4dpf (Fig. 5B). Altogether,
234 these observations are consistent with the epigenomic characterization based on retinal datasets and
235 provides further evidence of a potential *cis*-regulatory role of this UCNE on *PAX6* expression. Using the
236 same setting, we also evaluated the reported expression activity the mutated version of this UCNE,
237 i.e., harboring the SNV identified in the affected individuals of the family described before. However,
238 no conclusive differences were observed with respect to the wild-type version. A detailed overview of
239 the results of these assays can be found in Supplementary Table 10.

240 ## DISCUSSION

241 Since the landmark study of Bejerano et al. (Bejerano et al., 2004) almost twenty years ago,
242 ultraconservation of non-coding elements and their paradoxical functional (in)dispensability (Ahituv et
243 al., 2007; Chiang et al., 2008; Dickel et al., 2018; Drake et al., 2006; Snetkova, Pennacchio, et al., 2021)
244 have equally stirred controversy and fascination among scientists from diverse disciplines. A recent
245 study demonstrated that UCNEs with robust enhancer activity during embryonic development appear
246 to be unexpectedly resilient to mutation (Snetkova, Pennacchio, et al., 2021). There are, however, clear
247 instances in which variation within ultraconserved CREs can be a driver of human rare disease (Benko
248 et al., 2009; Bhatia et al., 2013; Ghiasvand et al., 2011; Klopocki et al., 2008; Kvon et al., 2020; Lettice
249 et al., 2003; Martínez et al., 2010; Plaisancié et al., 2018; Wieczorek et al., 2010). Despite the
250 substantial body of literature on these intriguing elements, thus far there are no comprehensive
251 studies based on the integration of multi-omics to map the regulatory capacity of UCNEs in a specific
252 tissue or cells, and on human genetic data to assess their contribution to disease. Apart from a few
253 well-known examples, variants in CREs are an underrepresented cause of Mendelian diseases. A major
254 obstacle hampering their identification is the need to define the search space of the CREs they affect
255 in a tissue- and even cell-type specific manner. Here we set out to address this challenge in human
256 retina, of which the *cis*-regulatory architecture has been well-studied (Cherry et al., 2020; Marchal et

al., 2022; Thomas et al., 2022) and for which there is emerging *cis*-regulatory variation implicated in disease (Bhatia et al., 2013; Ghiasvand et al., 2011; Plaisancié et al., 2018; Van de Sompele et al., 2022).

Although ENCODE provides a well-annotated inventory of cCREs, its retinal datasets do not include the earliest stages of RPC differentiation. To overcome this and to incorporate cell-type specificity information, we integrated scATAC-seq, which allowed us to identify 1,487 UCNEs characterized by accessible chromatin in at least one major stage of retinal development. We also interrogated the epigenetic landscape of these elements by analyzing histone modification patterns associated with e.g. active/poised enhancers (H3K27ac, H3K4me1, H3K4me2) (Creyghton et al., 2010; Rada-Iglesias et al., 2011; Santos-Rosa et al., 2002) and highly packed chromatin (H3K27me2 and H3K27me3) (Juan et al., 2016). This analysis provided a useful approach to trace the activity of elements that are active at a specific stage during retinal development. In total, 111 UCNEs were found to display active enhancer marks during retinal development. Similarly to ENCODE, the analyzed ChIP-seq datasets do not cover the earliest stages and hence these 111 elements are more likely to be related to stages of differentiation corresponding to later-born cell types (i.e., rod photoreceptors, bipolar cells, Müller glial, and some varieties of amacrine cells) (Rapaport et al., 2004). Interestingly, of these 111 elements, 33 were found to exhibit sustained enhancer-related signatures in adult stage, suggesting their potential role in the maintenance of gene expression patterns after development. Overall, our data integration spans all the major stages of retinogenesis and thus provides a comprehensive framework for the systematic characterization of ultraconserved retinal CREs.

Establishing an association between cCREs and their putative target genes is essential for the interpretation of genomic variation that could disrupt cell type-specific binding sites of TFs and/or long-range chromatin contacts that can lead to ectopic expression of genes (de Bruijn et al., 2020; Lupiáñez et al., 2015). Here we combined *GREAT* (McLean et al., 2010) with retinal expression and Hi-C derived retinal data to assign a range of action to candidate *cis*-regulatory UCNEs. We found this procedure to be more comprehensive than assigning target genes only based on the correlation provided by the peak-to-gene linkage method we used (Granja et al., 2021). In total, 594 retina-expressed genes can

be under UCNE *cis*-regulation; interestingly most of the UCNEs were found to be distributed in distal position from the TSS of their assigned target genes, as observed for enhancers promoting expression of developmental genes (Benko et al., 2009; Long et al., 2020; Pachano et al., 2022). In this regard, a large fraction of the identified ultraconserved putative enhancers clusters around key developmental genes (e.g. *MAB21L2*, *OTX2*, *PAX6*, *SOX2*, *ZEB2*) known to be controlled by complex regulatory landscapes (Polychronopoulos et al., 2017). Besides, 45 of these genes are implicated in rare eye diseases. Interestingly, coding variants in these genes lead in most cases to syndromic developmental phenotypes with other manifestations apart from the ocular ones as collated in the G2P database [23]. As it has been shown before, the phenotype caused by a coding mutation of a developmental gene can be different from the phenotype caused by a mutation in a CRE controlling spatiotemporal expression of this gene; this is exemplified by the *PRDM13* locus, for which bi-allelic coding *PRDM13* variants result in hypogonadotropic hypogonadism and perinatal brainstem dysfunction in combination with cerebellar hypoplasia (Whittaker et al., 2021) while *cis*-regulatory variants in retinal CREs leads to NCMD, a developmental macular disease (Van de Sompele et al., 2022). From our analyses we could identify a cCRE for *PRDM13* (*PRDM13_Blooklyn*) that displays an open chromatin context in early RPCs and developing amacrine cells, which are precisely the retinal cell types in which *PRDM13* is expressed (Goodson et al., 2018; Watanabe et al., 2015). Although no disease associations have been established thus far for other genes for which we identified candidate *cis*-regulatory UCNEs, some of them are known to play important roles in retina development, e.g., *NFIB* (Clark et al., 2019), and therefore represent potential target regions for non-coding variants contributing to missing heritability.

A limitation of this analysis is the usage of a pre-defined set of genomic regions, in particular UCNEs, as this database is static and rarely updated (Polychronopoulos et al., 2017). Our approach could thus be expanded using more flexible criteria, thus including other less conserved, albeit disease-relevant loci (Ghiasvand et al., 2011). Nonetheless, the advantage of working with highly conserved genomic regions is the availability of already validated experimental data (Visel et al., 2007); additionally, as

shown here, the integration of tissue-specific epigenomic data provides a robust framework to identify potential *bona fide* enhancers and their corresponding target genes, and clinically relevant variants therein.

To further investigate the contribution of genomic variation within candidate *cis*-regulatory UCNEs to disease, we mined WGS data from a sub-cohort of 100,000 Genome Project Genomics England participants affected by different rare eye diseases. As reported previously (Katzman et al., 2007; Snetkova, Pennacchio, et al., 2021), we observed a substantial depletion of common variation across these regions when compared to a background comprising randomly selected genomic regions. Indeed, intolerance to variation was also found to extend to the regions flanking the ones strictly defined as UCNEs. This apparently strong purifying selection has been proven difficult to reconcile with recent findings demonstrating remarkable resilience of UCNEs to variation (Snetkova, Ypsilanti, et al., 2021). Moreover, it has been suggested that weaker but uniform levels of purifying selection across hundreds of bases and different species could bring together these otherwise contradictory observations and explain why rare variants are not significantly depleted within UCNEs (Dukler et al., 2022). Our primary search space for variants with potential functional effects comprised 178 ultrarare variants located within 84 putatively active UCNEs associated with 29 genes. Interestingly, most of them were predicted to have a likely functional and/or deleterious effect, which could be explained by a skewed cumulative importance towards evolutionary conservation-related features in the predictive models (Rogers et al., 2018; Schwarz et al., 2019; Shi et al., 2021; Zhou & Troyanskaya, 2015).

Out of all variants found, one ultrarare variant (chr11:31968001T>C) within a UCNE displaying open chromatin in progenitor ganglion cells and linked to *PAX6* was further dissected. This variant was exclusively found within the studied family, displaying isolated foveal abnormalities, and initially solved with an ultrarare missense variant in *CFH*, which could not fully explain the clinical presentation (Raychaudhuri et al., 2011; Taylor et al., 2019). As no other likely pathogenic variants were found within relevant loci (Ehrenberg et al., 2021; Kuht et al., 2020, 2022; Small et al., 2016; Van de Sompele et al., 2022), and the observed phenotypes of the affected individuals match within the *PAX6* disease

spectrum, mis-regulation of *PAX6* expression cannot be excluded as a pathogenetic mechanism. Genetic defects of *PAX6* have been found in aniridia, a pan-ocular disorder characterized by the absence or hypoplasia of the iris, nystagmus and foveal hypoplasia (Cunha et al., 2019), the latter comprising thinning of macular inner and outer retinal layers consistent with misdirected foveal development (Pedersen et al., 2020). Recently, a phenotype characterized by isolated foveal hypoplasia with nystagmus has been also linked to *PAX6* variation (Lima Cunha et al., 2021). Given the known inter- and intra-familial phenotypic variability observed in *PAX6*-associated disorders (Dubey et al., 2015; Yokoi et al., 2016), variable expressivity cannot be discarded for the identified variant. Thus far, in terms of regulatory variation in CREs, only a single SNV located within the ultraconserved SIMO element has been associated with *PAX6*-disease. This subtle change (SNV), identified *de novo* in an individual with aniridia and foveal hypoplasia, was found to disrupt an autoregulatory PAX6 binding site (Bhatia et al., 2013). Importantly, we could establish *in vivo*, using the zebrafish as animal model, a developmental expression pattern in the eye driven by this UCNE in tissues for which *PAX6* expression is relevant (Ashery-Padan et al., 2000; Collinson et al., 2003; Georgala et al., 2011; Kimura et al., 2005; Pituello et al., 1999) and within a time window consistent with the period in which the zebrafish retina has become fully laminated (Morris & Fadool, 2005; Schmitt & Dowling, 1999). We could not obtain conclusive functional results for the identified variant using our experimental approach. A major limitation of this setting is the fact that the UCNE and its mutant version were tested outside of their native genomic context. Therefore, to validate the role of this UCNE in *PAX6* regulation, further functional assays that consider the native context, such as CRISPRi (Larson et al., 2013), are needed. Studying the molecular consequences of the variant itself in a patient-derived cellular model, however, is more challenging, since currently no models, including patient-derived retinal organoids, fully recapitulate foveal patterning (Hussey et al., 2022).

Overall, our work is exemplar for how the wealth of publicly available multi-omics data can be used to exploit the regulatory capacity of UCNEs in a tissue- and cell type-specific way. As demonstrated here, UCNEs can represent understudied regions of non-coding variation underlying missing heritability in

Mendelian diseases. With the increasing implementation of WGS in rare disease research and diagnosis, the delineation of tissue and cell type-specific CREs will be a prerequisite to identify and fully interpret the pathogenic nature of non-coding variants. With this study, we have illustrated how the creation of a comprehensive set of functionally annotated UCNEs in a target tissue can represent a powerful initial strategy to narrow down the variant search space, particularly for developmental phenotypes.

METHODS

Integration of UCNEs with bulk and single-cell epigenomic, regulatory and transcriptional datasets from human developing and adult retina

The 4,351 genomic regions defined as UCNEs (Dimitrieva & Bucher, 2013) were used as the basis for the integration of multiple publicly available multi-omics datasets derived from embryonic and adult human retina. More specifically, to evaluate the potential function of UCNEs as *cis*-regulatory modules, we made use of DNase-seq (Abascal et al., 2020), ChIP-seq of histone modifications (Aldiri et al., 2017; Cherry et al., 2020), and single-cell (sc) ATAC-seq (Thomas et al., 2022) derived from retinal tissue collected at distinct stages of development. Furthermore, to correlate potential *cis*-regulatory activity with gene expression, we mined both bulk (Hoshino et al., 2017) and scRNA-seq (Thomas et al., 2022) generated at stages overlapping or extending the ones of the epigenomic datasets. Additionally, as a last layer of functional characterization, we integrated into our analyses the experimental data of the VISTA Enhancer Browser (Visel et al., 2007), which allows the classification of candidate regulatory elements based on *in vivo* enhancer reporter assays tested in transgenic mice at embryonic day 11.5 (Pennacchio et al., 2006). Supplementary Table 11 provides an overview of all used datasets.

Identification of candidate *cis*-regulatory UCNEs in retina

Data generated by scATAC-seq of embryonic (53, 59, 74, 78, 113, and 132 days) and adult (25, 50, and 54 years old) human retinal cells were obtained (GSE183684) and imported into R (v4.0.5). Count

matrices were processed using the *ArchR* single-cell analysis package (v1.0.1) (Granja et al., 2021) as described in Thomas et al., 2022(Thomas et al., 2022) with minor modifications. Briefly, the total number of cells after filtering out doublets was 61,313. Single-nucleus RNA-seq of the same tissue and timepoints (GSE183684) were integrated using the unconstrained integration method so as to establish a linkage between the scATAC-seq and scRNA-seq datasets. More specifically, the unconstrained integration is a completely agnostic approach considering all cells derived from an scATAC-seq experiment and attempting to align them to any cells in the respective scRNA-seq experiment (Granja et al., 2021).

Both datasets were then used to assign retinal cell class identities to the different clusters based on known markers (Thomas et al., 2022) and subsequent peak calling. BigWig files from each annotated cell cluster were extracted and converted into bedGraph files using *bigWigtoBedGraph* UCSC utility; narrow peak detection was performed using *bdgpeakcall* (MACS2.2.7.1) (Y. Zhang et al., 2008) with default parameters and a value of 0.4 as cut-off (median peak width: 300bp). Similarly, bigWig files corresponding to histone modification patterns (H3K27Ac, H3K27me3, H3K36me3, H3K4me1, H3K4me2, H3K4me3, H3K9/14Ac, H3K9me3, PolII, CTCF) were retrieved (GSE87064) and converted into bedGraph files; in this case, the cut-off value for peak calling by *bdgpeakcall* was set at 20. Additionally, the subset of ENCODE DNase hypersensitivity sites (rDHSs) identified in embryonic retina (74-85, 89, 103-125 days) were obtained (ENCSR786VSQ, ENCSR666FML, ENCSR632UXV; median peak width: 300bp) and elements featured by *Low-DNase* filtered out.

Finally, to identify putative *cis*-regulatory UCNEs, we screened for overlaps between UCNEs and the retrieved sc-ATAC/ChIP/DNase-seq peaks using *bedtools intersect* (*BEDTools* v2.30.0)(Quinlan & Hall, 2010) with default parameters; of note *bedtools window* including a ±250bp-long window was used when overlapping the ChIP-seq peaks to characterize more broadly the chromatin status in the vicinity of the accessible UCNEs (Fig. S6).

Identification and characterization of target genes under putatively active UCNE regulation

To assign potential target genes to the identified active UCNEs we used the Genomic Regions Enrichment of Annotations Tool (*GREAT*) (McLean et al., 2010) (v4.0.4). Briefly, this tool computes statistics by associating genomic regions with nearby genes and applying the gene annotations to the regions. More specifically, when run against a whole genome background, two statistical tests are performed, namely the binomial test over genomic regions and the hypergeometric test over genes, thereby providing comprehensive annotation enrichments for the input genomic regions. Here, *GREAT* was run using an association rule based on the definition of an extended basal regulatory domain. Each gene in the genome was assigned a basal regulatory domain (5kb and 1kb upstream and downstream of the transcription start site {TSS}, respectively) with an extension of up to 1Mb to the nearest gene's basal domain. Each putatively active UCNE was then associated with all genes whose regulatory region it overlapped. In addition, curated regulatory domains were also included. These domain are supported by experimental evidence demonstrating that a gene is directly regulated by an element located beyond of its putative regulatory domain. In particular, for the utilized version of *GREAT*, these domains included the Sonic hedgehog long-range enhancer, the *HOXD* global control region, and the Beta-globin locus control region (McLean et al., 2010).

Potential target genes were subsequently filtered based on retinal expression. To do so, we retrieved RNA-seq paired-end FASTQ files derived from fetal retina samples (52 to 136 days post-conception) characterized in Hoshino et al. (Hoshino et al., 2017). Transcripts were quantified through pseudo-alignment by *Kallisto* (v.0.46.1)(Bray et al., 2016) using default parameters for both index build (derived from the Ensembl human release 101) and transcript abundance estimation. Transcript estimates were imported and summarized to create gene-level count matrices using *tximport* (v3.17) (Soneson et al., 2016). A custom script was then used to filter out target genes exhibiting no expression (TPM<0.5) at any of the interrogated stages. Additionally, to evaluate the reliability of the regulatory domains assigned by *GREAT* to these target genes, we integrated the 2,948 retinal TADs described by Marchal et al. (Marchal et al., 2022). To characterize further the putatively regulated target genes, we made use of the integration of the scATAC-seq gene scores and the scRNA-seq gene expression matrices

436 generated by *ArchR*. In particular, a gene score is a prediction of how highly expressed a gene will be
437 based on the accessibility of nearby regulatory elements (Granja et al., 2021). For each target gene, its
438 expression was ranked by percentile of expression across all clusters. A gene expression signature was
439 then assigned by retrieving the cluster identities exhibiting an expression value above the 80th
440 percentile threshold.

441 In addition, we compared the sets of target genes assigned to UCNEs by *GREAT* and subsequent gene
442 expression filtering, to those mapped using the peak-to-gene linkage method implemented by *ArchR*.
443 To do so, scATAC-seq data peaks that had a Peak2GeneLinkage correlation above 0.4 and their
444 corresponding target genes were kept. UCNES were then assigned to these peaks by *bedtools intersect*
445 as described above, including a ±250bp-long window The overlap between predicted target genes was
446 computed with respect to those assigned by *GREAT*.

447 Finally, to identify overrepresented Gene Ontology (GO) terms and infer possible enriched pathways
448 among the potential target genes under UCNE regulation, GO enrichment analyses were performed
449 using *Enrichr* (Xie et al., 2021).

450 **Interrogation of WGS data in a rare eye disease cohort**

451 Putatively active UCNEs associated with genes expressed in retina were filtered further based on their
452 implication in disease as retrieved from the comprehensive *gene-disease pairs and attributes* list
453 provided by G2P (Eye and Developmental Disease –DD– Panels; 2022-03-17) (Lenassi et al., 2021;
454 Thormann et al., 2019) extended with the NCMD-associated *IRX1* locus (Small et al., 2016). To assess
455 the contribution of genomic variation within these loci to disease, an analysis was performed to detect
456 small variants (SNVs, and indels < 50bp), and large structural variants (SVs) including copy number
457 variants (CNVs) overlapping these disease-gene associated UCNE loci through query of a sub-cohort of
458 participants with rare eye disease phenotypes (n = 3,220) from the 100,000 Genomes Project (100KGP,
459 Genomics England).

Retrieved variants were annotated with VEP (v.107). As a first filter, only variants with minor allele frequency (MAF) <0.5% and no observed homozygotes in gnomAD v3.1 were considered for further assessment. Variants were evaluated for their potential pathogenic/modifying effect using *in silico* prediction tools focusing on transcription factor (TF) binding site disruption -*QBiC-Pred*- and chromatin state effects -*DeepSea*, *CARMEN*, *FATHMM-XF*, *RegulationSpotter*- under default parameters (V. Martin et al., 2019; Rogers et al., 2018; Schwarz et al., 2019; Shi et al., 2021; Zhou & Troyanskaya, 2015). Furthermore, we annotated these variants with our integrated analyses in order to evaluate them within their regulatory context and potential target genes.

For each candidate variant, we compared the similarities between the participant phenotype (HPO terms) and the ones known for its target gene through literature search and clinical assessment by the recruiting clinician when possible. Finally, for each candidate variant identified in participants whose cases were not solved through 100KGP, a variant screening of 387 genes listed in either the Retinal disorders panel (v2.195) from Genomics England PanelApp (A. R. Martin et al., 2019) or RetNet (https://sph.uth.edu/retnet/) was performed to discard (likely) pathogenic variants, both SNVs and SVs, that could provide an alternative molecular diagnosis. For each instance for which only the UCNE variant remained as candidate, we placed a clinical collaboration request with Genomics England.

Evaluation of allele frequency distribution within UCNEs

Allele frequency distributions were created for the set of variants retrieved within disease-gene associated UCNE loci and compared against the distribution derived from a background composed of 200 random genomic sequences. This background was generated using the *random-genome-fragments* utility of Regulatory Sequence Analysis Tools (*RSAT*) with a fixed length of 350bp (Santana-Garcia et al., 2022). Importantly, *GREAT* was used to evaluate the distribution of distances of the randomly selected regions to the TSS of genes to ensure no confounding effects in the downstream analyses. Indeed, no significant differences were observed in such distribution as compared to that of the UCNEs (Fig. S1). Moreover, no GO terms were overrepresented among the target genes assigned

485 to these random genomic regions, thereby further supporting the suitability of this background for the
486 analysis.

487 To evaluate whether the depletion of common variation within UCNEs is a more general phenomenon,
488 we made use of genome-wide residual variation intolerance scores (gWRVIS), a nucleotide-resolution
489 metric that quantifies genomic constraint. As such, lower gwRVIS values correspond to greater
490 intolerance to variation (Vitsios et al., 2021). We downloaded gwRVIS data (hg38-build, v1.1) for all
491 chromosomes and queried it for the regions of interest using *tabix* (v1.7.2) (H. Li, 2011). More
492 specifically, these regions included: disease-gene associated UCNE loci, a flanking region encompassing
493 200bp up- and downstream of each of these UCNEs, and the 200 random genomic sequences
494 described above. Two-sided Mann–Whitney U tests were used to compare the gwRVIS distributions
495 across all pairs.

496 Additionally, in order to assess the specificity of the overlap of rare variants in the studied patient sub-
497 cohort with UCNEs, we generated allele frequency distributions corresponding to all variants retrieved
498 for a selection of 25 target disease gene loci under putative UCNE regulation and their corresponding
499 UCNEs. For each disease-gene and UCNE pair, we plotted the proportion of ultra-rare (absent from
500 gnomAD v3.1), very rare (MAF < 0.1%), rare (0.1% ≤ MAF < 0.5%), low frequency (0.5% ≤ MAF < 5%),
501 and common (MAF ≥ 5%) variants.

502 **Targeted sequencing and reverse phenotyping**

503 We performed segregation testing of two ultrarare SNVs initially identified in three affected individuals
504 of a 3-generation family displaying autosomal dominant foveal abnormalities, namely an SNV in a
505 candidate *cis*-regulatory UCNE located upstream of *PAX6* and a missense *CFH* variant. Genomic DNA
506 was extracted using Oragene-DNA saliva kits (OG-500, DNA Genotek) according to manufacturer's
507 instructions. Targeted sequencing of the variants was performed on genomic DNA by PCR amplification
508 followed by Sanger sequencing using the BigDye Terminator v3.1 kit (Life Technologies). Primer
509 sequences can be found in Supplementary Table 12.

Following their genetic assessment, four members of this 3-generation family were clinically re-evaluated. The examination included visual acuity assessment, slit-lamp examination for anterior and posterior segment anomalies, and intraocular pressure measurement. Detailed imaging involving ultra-wide field fundus photography, ultra-wide field autofluorescence imaging and optical coherence tomography (OCT) was performed.

Generation of *in vivo* reporter constructs and functional characterization of candidate *cis*-regulatory UCNE upstream of *PAX6* using enhancer assays in zebrafish embryos

Primers were designed to amplify the sequence of the candidate *cis*-regulatory UCNE located upstream of *PAX6* from human genomic DNA (Roche). The PCR product was then cloned into the E1b-GFP-Tol2 enhancer assay vector containing an E1b minimal promoter followed by the Green Fluorescent Protein (GFP) reporter gene(Q. Li et al., 2010) by restriction-ligation cloning. The primer sequences can be found in Supplementary Table 12. The recombinant vector containing the cCRE-*PAX6*-UCNE was then amplified in One Shot TOP10 Chemically Competent E. coli cells (Invitrogen) and purified using the QIAprep Spin Miniprep Kit (Qiagen). Additionally, a construct containing the ultra-rare SNV identified in the affected individuals of the family described above was created using the Q5 Site-Directed Mutagenesis Kit (NEB) using variant-specific primers designed with the NEBaseChanger tool. The sequence of the insert was confirmed by Sanger sequencing using the BigDye Terminator v3.1 kit (Life Technologies). The constructs were then microinjected into the yolk of at least 70 wild-type zebrafish embryos at single-cell stage using the Tol2 transposase system for germline integration of the transgene according to Bessa *et al*. (Bessa et al., 2009) with minor modifications. As readout, GFP fluorescence was observed and photographed with a Leica M165 FC Fluorescent Stereo Microscope (Leica Microsystems) and its localization annotated at 1, 2 and 3 days post fertilization (dpf) to evaluate enhancer activity.

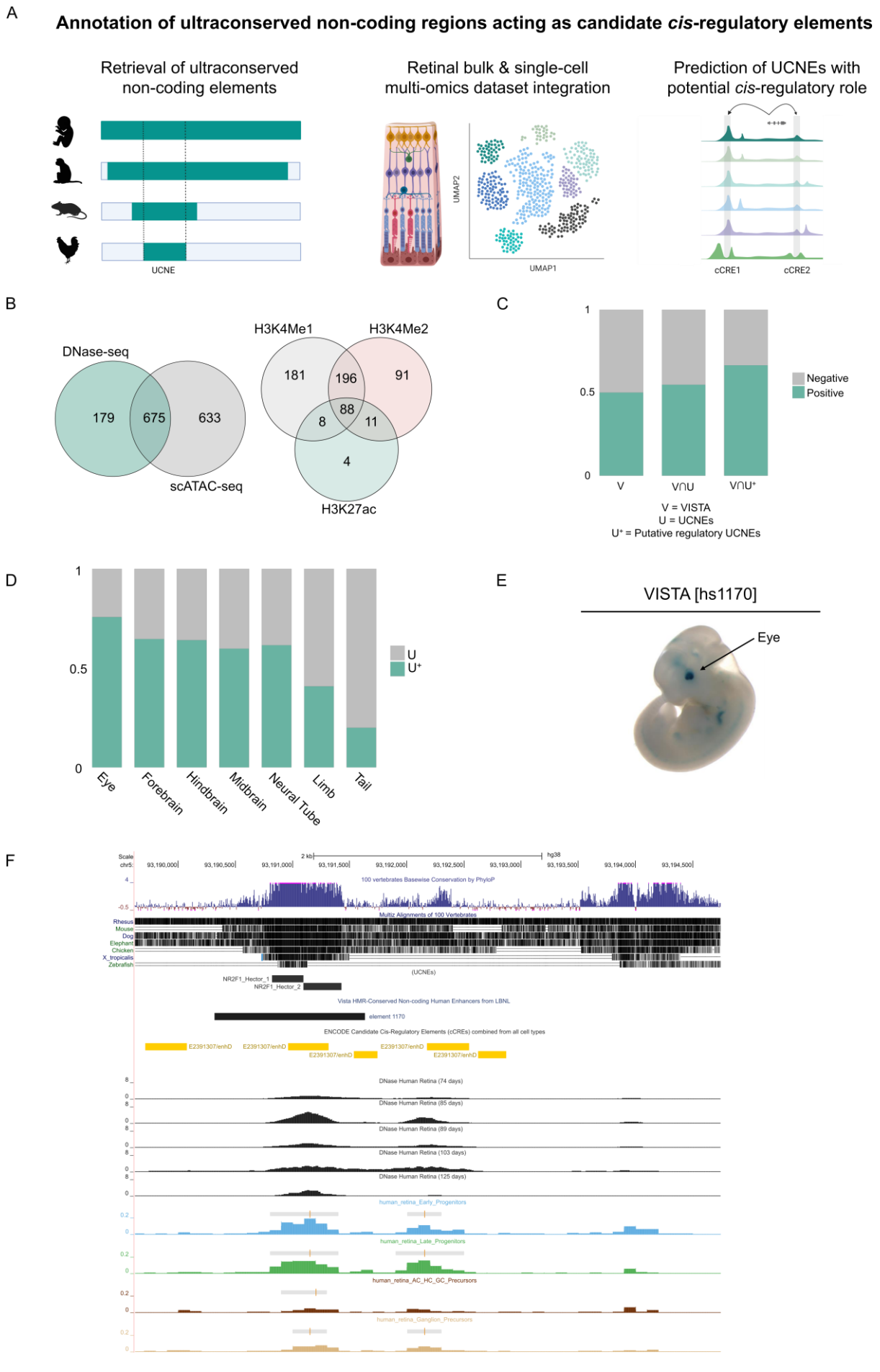

Figure 1. Integration of publicly available datasets for the characterization of the ultraconserved non-coding elements (UCNEs) library. A) Overview of the integrative multi-omics analysis for the prediction of UCNEs with potential *cis*-regulatory role in human retina. **B)** Venn diagrams illustrating the CREs displaying open chromatin features based on scATAC-seq and DNase-seq (left) and their overlap of active enhancer marks (H3K27ac, H3K4me1 and H3K4me2). **C)** Barplot showing the proportions of elements from the VISTA enhancer browser (V), UCNEs (U), and putative regulatory UCNEs (characterized by retinal datasets) (U^+) displaying reporter expression (positive). **D)** Proportional stacked barplot showing the distribution of tissues (eye, forebrain, hindbrain, midbrain, neural tube, limb and tail) in which the putative regulatory UCNEs display reporter expression. **E-F)** Illustration of one of the characterized UCNEs (NR2F1_Hector_1/2) displaying open chromatin supported by DNase-seq (embryonic day 74-85, 89 and 103-125) and scATAC-seq (AC/HC/GC Precursors Cells, Early Progenitor Cells, Ganglion Precursor Cells, Late Retinal Progenitor Cells) and enhancer reporter expression in the eye. Figures obtained from VISTA (hs1170) enhancer (E) and UCSC genome (F) browsers. Abbreviations: FW: fetal weeks; V: VISTA enhancer elements; U: UCNEs; U^+: Putative active regulatory UCNE; ∩: intersection.

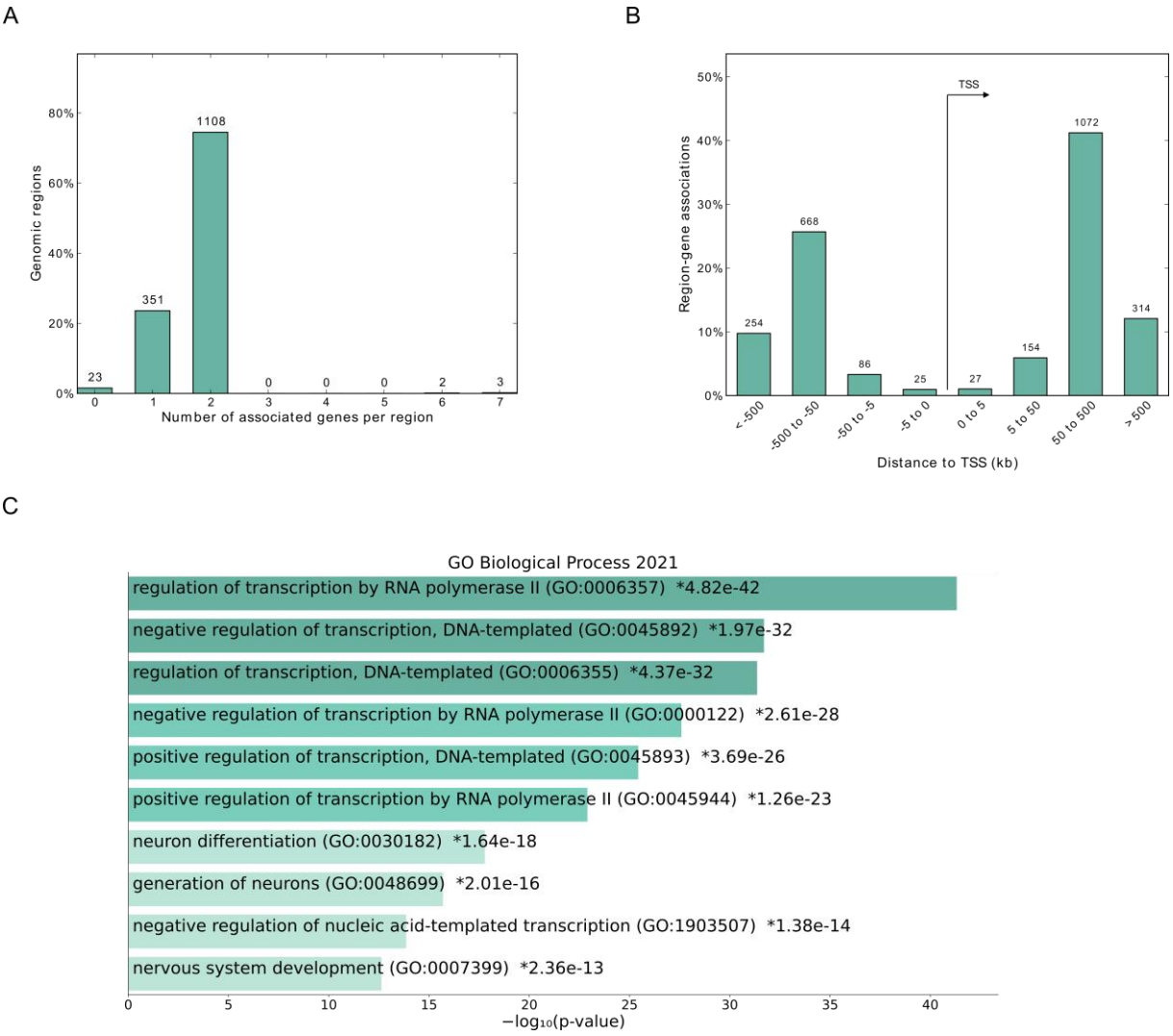

Figure 2. Target genes under putative regulation of characterized UCNEs in retina. A) Bar plot showing the number of associated genes per retinal UCNE. **B)** Distance distribution from the TSS and its associated UCNE. **C)** Gene ontology for the UCNE-associated target genes. Abbreviations: GO: Gene Ontology; TSS: transcription start site.

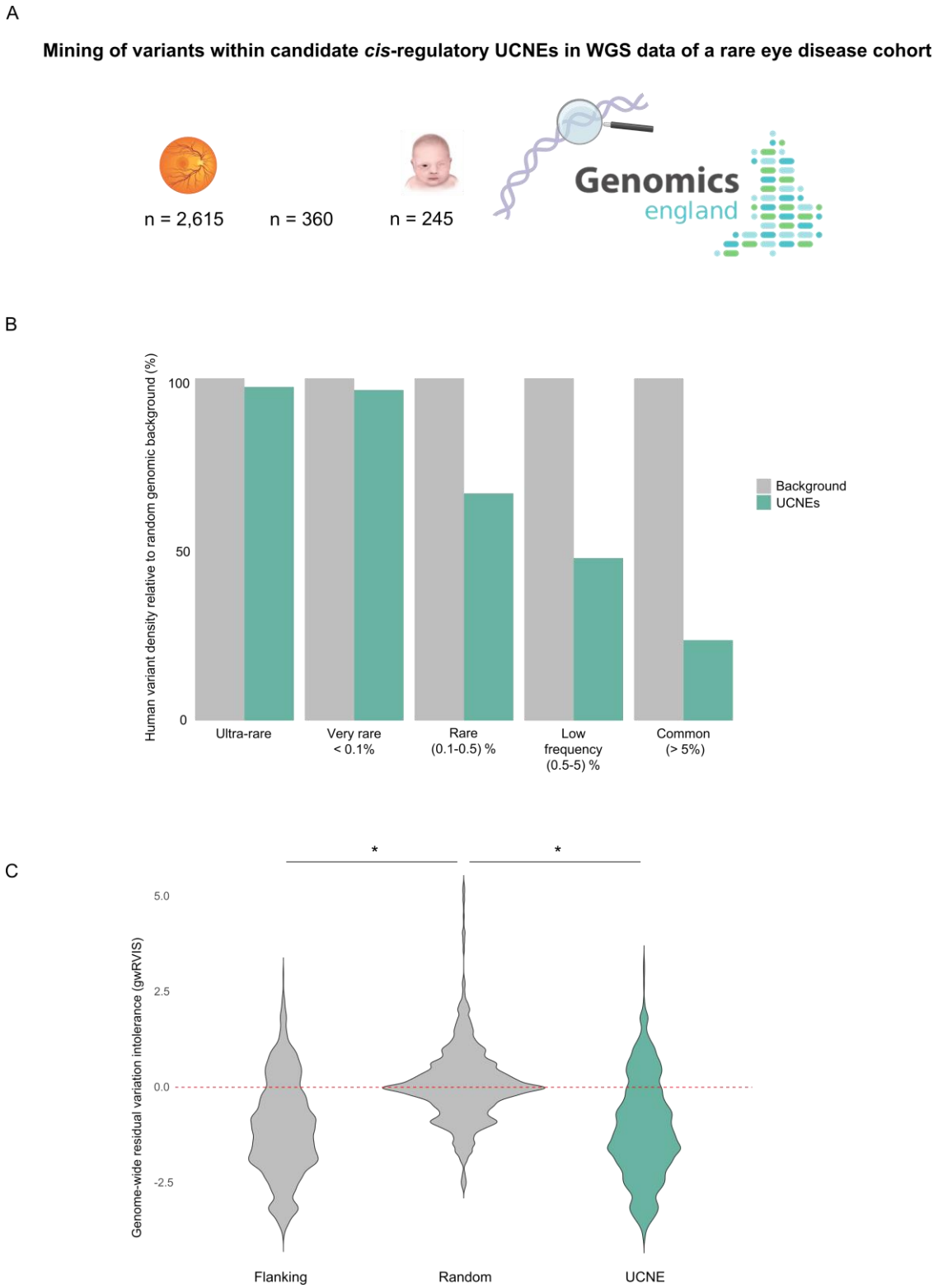

Figure 3. Contribution of UCNE genomic variation to missing heritability in rare eye diseases. A) Overview of a sub-cohort comprising n=3,220 participants of the 100,000 Genomes Project affected by posterior segment abnormalities (n=2,615), anterior segment abnormalities (n=360), and ocular malformations (n=245). **B)** Variant population frequencies within putative retinal UCNEs normalized to a background composed of randomly selected sequences (*see Methods*). **C)** Significantly lower genome-wide residual variation score (gwRVIS) values scores are observed across UCNEs and their flanking regions compared to the background composed randomly selected sequences, thereby showing the high intolerance to variation of UCNEs.

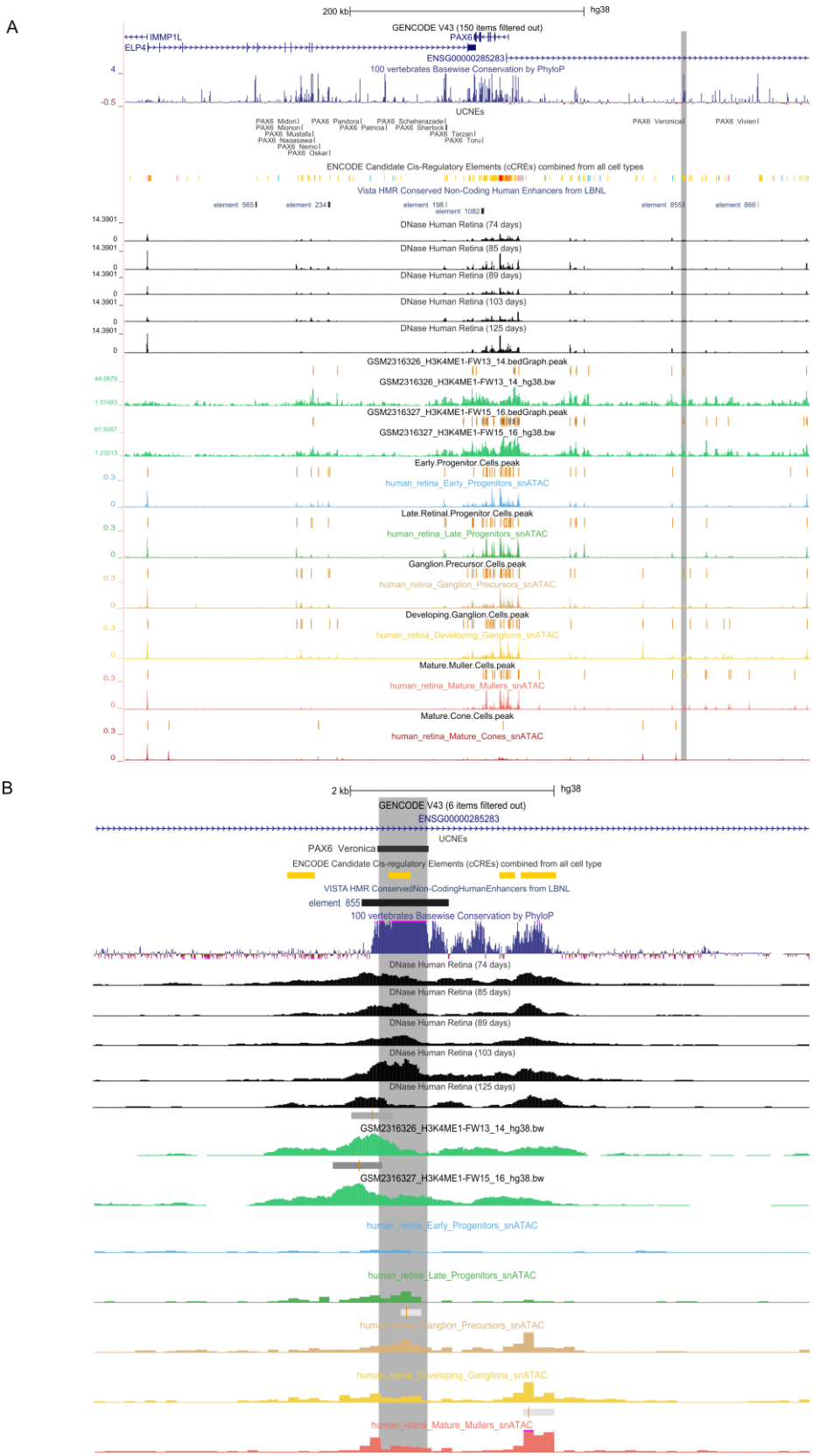

Figure 4. Characterization of the *cis*-regulatory landscape of *PAX6* in human retina. A) Visualization of the epigenomic context of the identified *PAX6*-associated UCNE (highlighted in *gray*) in relation to the *PAX6* locus (*top;* chr11:31,490,261-32,075,591) and **B)** Zoomed-in of the identified element (*bottom*; chr11:31,965,000-31,972,000). Figures are obtained from the UCSC genome browser.

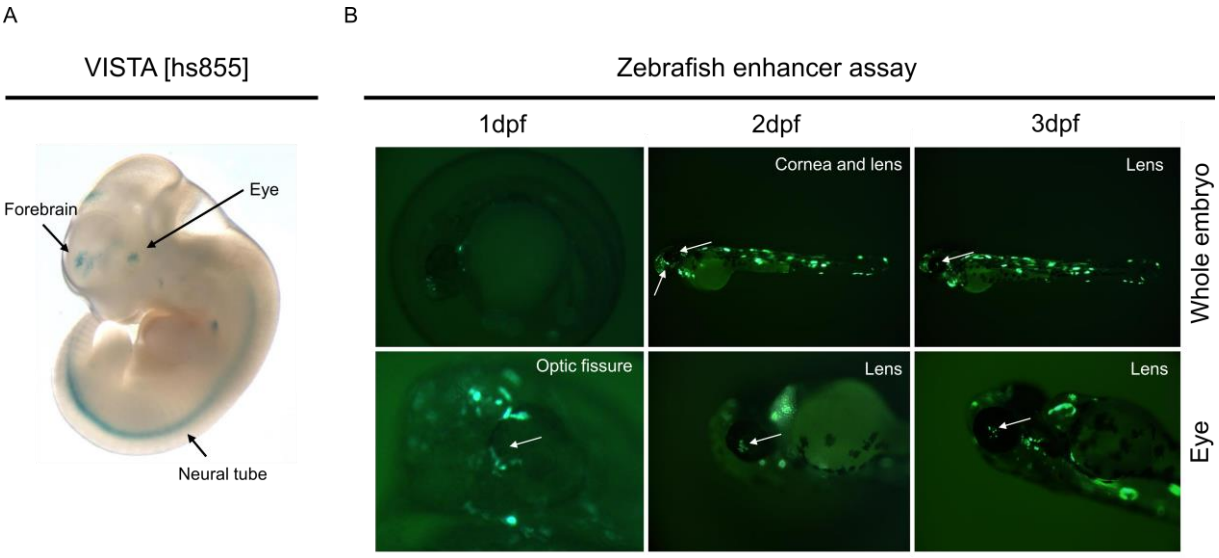

Figure 5. *In vivo* evaluation of the *PAX6*-associated UCNE. A) This UCNE displays reporter activity in the human embryonic forebrain (6/9 embryos) as well as in other structures including eye (3/6 embryos) and neural tube. Figure obtained from the VISTA enhancer browser (hs855). **B)** Zebrafish enhancer assays at 3 different time points (1 dpf, 2 dpf, 3 dpf) showing GFP-positive tissues (optic fissure -1 dpf-, lens cells -2,3 dpf- and forebrain -2,3 dpf-; *white arrows*). Abbreviations. dpf: days post-fertilization.

COMPETING INTEREST STATEMENT

The authors declare that they have no competing interests.

FUNDING

This work was supported by the Ghent University Special Research Fund (BOF20/GOA/023) (EDB); H2020 MSCA ITN grant (No. 813490 StarT) (EDB, FC, MB), EJPRD19-234 Solve-RET (EDB). EDB is a Senior Clinical Investigator (1802220N) of the Research Foundation-Flanders (FWO); VLS and ADR are an Early Starting Researcher of StarT (grant No. 813490). EDB is member of ERN-EYE (Framework Partnership Agreement No 739534-ERN-EYE).

ACKNOWLEDGEMENTS

This research was made possible through access to the data and findings generated by the 100,000 Genomes Project. The 100,000 Genomes Project is managed by Genomics England Limited (a wholly owned company of the Department of Health and Social Care). The 100,000 Genomes Project is funded by the National Institute for Health Research and NHS England. The Welcome Trust, Cancer Research UK and the Medical Research Council have also funded research infrastructure. The 100,000 Genomes Project uses data provided by patients and collected by the National Health Service as part of their care and support. We acknowledge Chris Inglehearn (Leeds Institute of Medical Research, School of Medicine, University of Leeds, Leeds, UK) for his helpful advice and comments for the manuscript. We also would like to thank the Zebrafish Facility Ghent (ZFG) Core at Ghent University. Hanna De Saffel, Quinten Mahieu, Angelika Jürgens and Lies Vantomme are thanked for their excellent technical assistance.

ETHICS APPROVAL AND CONSENT TO PARTICIPATE

The 100,000 Genomes Project Protocol has ethical approval from the HRA Committee East of England – Cambridge South (REC Ref 14/EE/1112). This study was registered with Genomics England under Research Registry Projects 465.

AUTHORS' CONTRIBUTIONS

V.L.S.: Conception and project design, acquisition of data, analysis and interpretation of data, drafting and revising the manuscript.

A.D.R.: Conception and project design, acquisition of data, analysis and interpretation of data, drafting and revising the manuscript.

R.M: Acquisition of data, analysis and interpretation of data, revising the manuscript.

G.E: Acquisition of data, revising the manuscript.

F.C: Acquisition of data, revising the manuscript.

M.B: Project supervision, acquisition of data, revising the manuscript.

A.W: Acquisition of data, analysis and interpretation of data, revising the manuscript.

E.D.B.: Conception and project supervision, acquisition of data, analysis and interpretation of data, drafting and revising the manuscript.

CONSENT FOR PUBLICATION

Not applicable. We present only de-identified data.

AVAILABILITY OF DATA AND MATERIALS

The data that support the findings of this study are available within the Genomics England (protected) Research Environment but restrictions apply to the availability of these data, as access to the Research Environment is limited to protect the privacy and confidentiality of participants. De-identified data as well as analysis scripts are, however, available from the authors upon reasonable request. Extended data generated in this study are available in the supplementary materials.

REFERENCES

Abascal, F., Acosta, R., Addleman, N. J., Adrian, J., Afzal, V., Aken, B., Akiyama, J. A., Jammal, O. Al, … Zimmerman, J. (2020). Expanded encyclopaedias of DNA elements in the human and mouse genomes. *Nature*, *583*(7818), 699–710. https://doi.org/10.1038/s41586-020-2493-4

Ahituv, N., Zhu, Y., Visel, A., Holt, A., Afzal, V., Pennacchio, L. A., & Rubin, E. M. (2007). Deletion of ultraconserved elements yields viable mice. *PLoS Biology*, *5*(9), 1906–1911. https://doi.org/10.1371/journal.pbio.0050234

Aldiri, I., Xu, B., Wang, L., Chen, X., Hiler, D., Griffiths, L., Valentine, M., Shirinifard, A., … Dyer, M. A. (2017). The Dynamic Epigenetic Landscape of the Retina During Development, Reprogramming, and Tumorigenesis. *Neuron*, *94*(3), 550-568.e10. https://doi.org/10.1016/j.neuron.2017.04.022

Ashery-Padan, R., Marquardt, T., Zhou, X., & Gruss, P. (2000). Pax6 activity in the lens primordium is required for lens formation and for correct placement of a single retina in the eye. *Genes and Development*, *14*(21), 2701–2711. https://doi.org/10.1101/gad.184000

Bejerano, G., Pheasant, M., Makunin, I., Stephen, S., Kent, W. J., Mattick, J. S., & Haussler, D. (2004). Ultraconserved elements in the human genome. *Science*, *304*(5675), 1321–1325. https://doi.org/10.1126/science.1098119

Benko, S., Fantes, J. A., Amiel, J., Kleinjan, D. J., Thomas, S., Ramsay, J., Jamshidi, N., Essafi, A., … Lyonnet, S. (2009). Highly conserved non-coding elements on either side of SOX9 associated with Pierre Robin sequence. *Nature Genetics*, *41*(3), 359–364. https://doi.org/10.1038/ng.329

Bessa, J., Tena, J. J., De La Calle-Mustienes, E., Fernández-Miñán, A., Naranjo, S., Fernández, A., Montoliu, L., Akalin, A., … Gómez-Skarmeta, J. L. (2009). Zebrafish Enhancer Detection (ZED) vector: A new tool to facilitate transgenesis and the functional analysis of cis-regulatory regions in zebrafish. *Developmental Dynamics*, *238*(9), 2409–2417. https://doi.org/10.1002/dvdy.22051

Bhatia, S., Bengani, H., Fish, M., Brown, A., Divizia, M. T., De Marco, R., Damante, G., Grainger, R., … Kleinjan, D. A. (2013). Disruption of autoregulatory feedback by a mutation in a remote, ultraconserved PAX6 enhancer causes aniridia. *American Journal of Human Genetics*, *93*(6), 1126–1134. https://doi.org/10.1016/j.ajhg.2013.10.028

Bray, N. L., Pimentel, H., Melsted, P., & Pachter, L. (2016). Near-optimal probabilistic RNA-seq quantification. *Nature Biotechnology*, *34*(5), 525–527. https://doi.org/10.1038/nbt.3519

Cherry, T. J., Yang, M. G., Harmin, D. A., Tao, P., Timms, A. E., Bauwens, M., Allikmets, R., Jones, E. M., … Greenberg, M. E. (2020). Mapping the cis-regulatory architecture of the human retina reveals noncoding genetic variation in disease. *Proceedings of the National Academy of Sciences of the United States of America*, *117*(16), 9001–9012. https://doi.org/10.1073/pnas.1922501117

Chiang, C. W. K., Derti, A., Schwartz, D., Chou, M. F., Hirschhorn, J. N., & Wu, C. T. (2008). Ultraconserved elements: Analyses of dosage sensitivity, motifs and boundaries. *Genetics*, *180*(4), 2277–2293. https://doi.org/10.1534/genetics.108.096537

Cipriani, V., Silva, R. S., Arno, G., Pontikos, N., Kalhoro, A., Valeina, S., Inashkina, I., Audere, M., … Moore, A. T. (2017). Duplication events downstream of IRX1 cause North Carolina macular dystrophy at the MCDR3 locus. *Scientific Reports*, *7*(1), 1–9. https://doi.org/10.1038/s41598-017-06387-6

Clark, B. S., Stein-O'Brien, G. L., Shiau, F., Cannon, G. H., Davis-Marcisak, E., Sherman, T., Santiago, C. P., Hoang, T. V., … Blackshaw, S. (2019). Single-Cell RNA-Seq Analysis of Retinal Development Identifies NFI Factors as Regulating Mitotic Exit and Late-Born Cell Specification. *Neuron*, *102*(6), 1111-1126.e5. https://doi.org/10.1016/j.neuron.2019.04.010

679 Collinson, J. M., Quinn, J. C., Hill, R. E., & West, J. D. (2003). The roles of Pax6 in the cornea, retina,
680 and olfactory epithelium of the developing mouse embryo. *Developmental Biology*, *255*(2),
681 303–312. https://doi.org/10.1016/S0012-1606(02)00095-7

682 Creyghton, M. P., Cheng, A. W., Welstead, G. G., Kooistra, T., Carey, B. W., Steine, E. J., Hanna, J.,
683 Lodato, M. A., … Jaenisch, R. (2010). Histone H3K27ac separates active from poised enhancers
684 and predicts developmental state. *Proceedings of the National Academy of Sciences of the*
685 *United States of America*, *107*(50), 21931–21936. https://doi.org/10.1073/pnas.1016071107

686 Cunha, D. L., Arno, G., Corton, M., & Moosajee, M. (2019). The spectrum of PAX6 mutations and
687 genotype-phenotype correlations in the eye. *Genes*, *10*(12).
688 https://doi.org/10.3390/genes10121050

689 de Bruijn, S. E., Fiorentino, A., Ottaviani, D., Fanucchi, S., Melo, U. S., Corral-Serrano, J. C., Mulders,
690 T., Georgiou, M., … Hardcastle, A. J. (2020). Structural Variants Create New Topological-
691 Associated Domains and Ectopic Retinal Enhancer-Gene Contact in Dominant Retinitis
692 Pigmentosa. *American Journal of Human Genetics*, *107*(5), 802–814.
693 https://doi.org/10.1016/j.ajhg.2020.09.002

694 Dickel, D. E., Ypsilanti, A. R., Pla, R., Zhu, Y., Barozzi, I., Mannion, B. J., Khin, Y. S., Fukuda-Yuzawa, Y.,
695 … Visel, A. (2018). Ultraconserved Enhancers Are Required for Normal Development. *Cell*,
696 *172*(3), 491-499.e15. https://doi.org/10.1016/j.cell.2017.12.017

697 Dimitrieva, S., & Bucher, P. (2013). UCNEbase - A database of ultraconserved non-coding elements
698 and genomic regulatory blocks. *Nucleic Acids Research*, *41*(D1), 101–109.
699 https://doi.org/10.1093/nar/gks1092

700 Dixon, J. R., Selvaraj, S., Yue, F., Kim, A., Li, Y., Shen, Y., Hu, M., Liu, J. S., & Ren, B. (2012). Topological
701 domains in mammalian genomes identified by analysis of chromatin interactions. *Nature*,
702 *485*(7398), 376–380. https://doi.org/10.1038/nature11082

703 Drake, J. A., Bird, C., Nemesh, J., Thomas, D. J., Newton-Cheh, C., Reymond, A., Excoffier, L., Attar, H.,
704 … Hirschhorn, J. N. (2006). Conserved noncoding sequences are selectively constrained and not
705 mutation cold spots. *Nature Genetics*, *38*(2), 223–227. https://doi.org/10.1038/ng1710

706 Dubey, S. K., Mahalaxmi, N., Vijayalakshmi, P., & Sundaresan, P. (2015). Mutational analysis and
707 genotype-phenotype correlations in southern Indian patients with sporadic and familial aniridia.
708 *Molecular Vision*, *21*(January), 88–97.

709 Dukler, N., Mughal, M. R., Ramani, R., Huang, Y. F., & Siepel, A. (2022). Extreme purifying selection
710 against point mutations in the human genome. *Nature Communications*, *13*(1).
711 https://doi.org/10.1038/s41467-022-31872-6

712 Dunham, I., Kundaje, A., Aldred, S. F., Collins, P. J., Davis, C. A., Doyle, F., Epstein, C. B., Frietze, S., …
713 Lochovsky, L. (2012). An integrated encyclopedia of DNA elements in the human genome.
714 *Nature*, *489*(7414), 57–74. https://doi.org/10.1038/nature11247

715 Ehrenberg, M., Bagdonite-Bejarano, L., Fulton, A. B., Orenstein, N., & Yahalom, C. (2021). Genetic
716 causes of nystagmus, foveal hypoplasia and subnormal visual acuity- other than albinism.
717 *Ophthalmic Genetics*, *42*(3), 243–251. https://doi.org/10.1080/13816810.2021.1888128

718 Ellingford, J. M., Barton, S., Bhaskar, S., O'Sullivan, J., Williams, S. G., Lamb, J. A., Panda, B.,
719 Sergouniotis, P. I., … Black, G. C. M. (2016). Molecular findings from 537 individuals with
720 inherited retinal disease. *Journal of Medical Genetics*, *53*(11), 761–767.
721 https://doi.org/10.1136/jmedgenet-2016-103837

722 Engström, P. G., Fredman, D., & Lenhard, B. (2008). Ancora: A web resource for exploring highly

conserved noncoding elements and their association with developmental regulatory genes. *Genome Biology*, *9*(2), 8–11. https://doi.org/10.1186/gb-2008-9-2-r34

Field, A., & Adelman, K. (2020). Evaluating Enhancer Function and Transcription. *Annual Review of Biochemistry*, *89*, 213–234. https://doi.org/10.1146/annurev-biochem-011420-095916

Georgala, P. A., Carr, C. B., & Price, D. J. (2011). The role of Pax6 in forebrain development. *Developmental Neurobiology*, *71*(8), 690–709. https://doi.org/10.1002/dneu.20895

Ghiasvand, N. M., Rudolph, D. D., Mashayekhi, M., Brzezinski, J. A., Goldman, D., & Glaser, T. (2011). Deletion of a remote enhancer near ATOH7 disrupts retinal neurogenesis, causing NCRNA disease. *Nature Neuroscience*, *14*(5), 578–588. https://doi.org/10.1038/nn.2798

Goodson, N. B., Nahreini, J., Randazzo, G., Uruena, A., Johnson, J. E., & Brzezinski, J. A. (2018). Prdm13 is required for Ebf3+ amacrine cell formation in the retina. *Developmental Biology*, *434*(1), 149–163. https://doi.org/10.1016/j.ydbio.2017.12.003

Granja, J. M., Corces, M. R., Pierce, S. E., Bagdatli, S. T., Choudhry, H., Chang, H. Y., & Greenleaf, W. J. (2021). Author Correction: ArchR is a scalable software package for integrative single-cell chromatin accessibility analysis (Nature Genetics, (2021), 53, 3, (403-411), 10.1038/s41588-021-00790-6). *Nature Genetics*, *53*(6), 935. https://doi.org/10.1038/s41588-021-00850-x

Haer-Wigman, L., Van Zelst-Stams, W. A. G., Pfundt, R., Van Den Born, L. I., Klaver, C. C. W., Verheij, J. B. G. M., Hoyng, C. B., Breuning, M. H., … Yntema, H. G. (2017). Diagnostic exome sequencing in 266 Dutch patients with visual impairment. *European Journal of Human Genetics*, *25*(5), 591–599. https://doi.org/10.1038/ejhg.2017.9

Hoshino, A., Ratnapriya, R., Brooks, M. J., Chaitankar, V., Wilken, M. S., Zhang, C., Starostik, M. R., Gieser, L., … Reh, T. A. (2017). Molecular Anatomy of the Developing Human Retina. *Developmental Cell*, *43*(6), 763-779.e4. https://doi.org/10.1016/j.devcel.2017.10.029

Hussey, K. A., Hadyniak, S. E., & Johnston, R. J. (2022). Patterning and Development of Photoreceptors in the Human Retina. *Frontiers in Cell and Developmental Biology*, *10*(April), 1–21. https://doi.org/10.3389/fcell.2022.878350

Juan, A. H., Wang, S., Ko, K. D., Zare, H., Tsai, P. F., Feng, X., Vivanco, K. O., Ascoli, A. M., … Sartorelli, V. (2016). Roles of H3K27me2 and H3K27me3 Examined during Fate Specification of Embryonic Stem Cells. *Cell Reports*, *17*(5), 1369–1382. https://doi.org/10.1016/j.celrep.2016.09.087

Katzman, S., Kern, A. D., Bejerano, G., Fewell, G., Fulton, L., Wilson, R. K., Salama, S. R., & Haussler, D. (2007). Human genome ultraconserved elements are ultraselected. *Science*, *317*(5840), 915. https://doi.org/10.1126/science.1142430

Kimura, J., Suda, Y., Kurokawa, D., Hossain, Z. M., Nakamura, M., Takahashi, M., Hara, A., & Aizawa, S. (2005). Emx2 and Pax6 function in cooperation with Otx2 and Otx1 to develop caudal forebrain primordium that includes future archipallium. *Journal of Neuroscience*, *25*(21), 5097–5108. https://doi.org/10.1523/JNEUROSCI.0239-05.2005

Klopocki, E., Ott, C. E., Benatar, N., Ullmann, R., Mundlos, S., & Lehmann, K. (2008). A microduplication of the long range SHH limb regulator (ZRS) is associated with triphalangeal thumb-polysyndactyly syndrome. *Journal of Medical Genetics*, *45*(6), 370–375. https://doi.org/10.1136/jmg.2007.055699

Kuht, H. J., Han, J., Maconachie, G. D. E., Park, S. E., Lee, S. T., McLean, R., Sheth, V., Hisaund, M., … Thomas, M. G. (2020). SLC38A8 mutations result in arrested retinal development with loss of cone photoreceptor specialization. *Human Molecular Genetics*, *29*(18), 2989–3002. https://doi.org/10.1093/hmg/ddaa166

767 Kuht, H. J., Maconachie, G. D. E., Han, J., Kessel, L., van Genderen, M. M., McLean, R. J., Hisaund, M.,
768 Tu, Z., … Thomas, M. G. (2022). Genotypic and Phenotypic Spectrum of Foveal Hypoplasia: A
769 Multicenter Study. *Ophthalmology*, *129*(6), 708–718.
770 https://doi.org/10.1016/j.ophtha.2022.02.010

771 Kvon, E. Z., Zhu, Y., Kelman, G., Novak, C. S., Plajzer-Frick, I., Kato, M., Garvin, T. H., Pham, Q., …
772 Pennacchio, L. A. (2020). Comprehensive In Vivo Interrogation Reveals Phenotypic Impact of
773 Human Enhancer Variants. *Cell*, *180*(6), 1262-1271.e15.
774 https://doi.org/10.1016/j.cell.2020.02.031

775 Larson, M. H., Gilbert, L. A., Wang, X., Lim, W. A., Weissman, J. S., & Qi, L. S. (2013). CRISPR
776 interference (CRISPRi) for sequence-specific control of gene expression. *Nature Protocols*,
777 *8*(11), 2180–2196. https://doi.org/10.1038/nprot.2013.132

778 Lenassi, E., Carvalho, A., Thormann, A., Fletcher, T., Hardcastle, C., Hunt, S. E., Sergouniotis, P. I.,
779 Michaelides, M., … Ellingford, J. M. (2021). EyeG2P: an automated variant filtering approach
780 improves efficiency of diagnostic genomic testing for inherited ophthalmic disorders. *MedRxiv*,
781 2021.07.23.21261017.
782 https://www.medrxiv.org/content/10.1101/2021.07.23.21261017v1%0Ahttps://www.medrxiv.
783 org/content/10.1101/2021.07.23.21261017v1.abstract

784 Lettice, L. A., Heaney, S. J. H., Purdie, L. A., Li, L., de Beer, P., Oostra, B. A., Goode, D., Elgar, G., … de
785 Graaff, E. (2003). A long-range Shh enhancer regulates expression in the developing limb and fin
786 and is associated with preaxial polydactyly. *Human Molecular Genetics*, *12*(14), 1725–1735.
787 https://doi.org/10.1093/hmg/ddg180

788 Li, H. (2011). Tabix: Fast retrieval of sequence features from generic TAB-delimited files.
789 *Bioinformatics*, *27*(5), 718–719. https://doi.org/10.1093/bioinformatics/btq671

790 Li, Q., Ritter, D., Yang, N., Dong, Z., Li, H., Chuang, J. H., & Guo, S. (2010). A systematic approach to
791 identify functional motifs within vertebrate developmental enhancers. *Developmental Biology*,
792 *337*(2), 484–495. https://doi.org/10.1016/j.ydbio.2009.10.019

793 Lima Cunha, D., Owen, N., Tailor, V., Corton, M., Theodorou, M., & Moosajee, M. (2021). PAX6
794 missense variants in two families with isolated foveal hypoplasia and nystagmus: evidence of
795 paternal postzygotic mosaicism. *European Journal of Human Genetics*, *29*(2), 349–355.
796 https://doi.org/10.1038/s41431-020-00737-1

797 Lomonaco, V., Martoglia, R., Mandreoli, F., Anderlucci, L., Emmett, W., Bicciato, S., & Taccioli, C.
798 (2014). UCbase 2.0: Ultraconserved sequences database (2014 update). *Database*, *2014*, 1–8.
799 https://doi.org/10.1093/database/bau062

800 Long, H. K., Osterwalder, M., Welsh, I. C., Hansen, K., Davies, J. O. J., Liu, Y. E., Koska, M., Adams, A.
801 T., … Wysocka, J. (2020). Loss of Extreme Long-Range Enhancers in Human Neural Crest Drives a
802 Craniofacial Disorder. *Cell Stem Cell*, *27*(5), 765-783.e14.
803 https://doi.org/10.1016/j.stem.2020.09.001

804 Lupiáñez, D. G., Kraft, K., Heinrich, V., Krawitz, P., Brancati, F., Klopocki, E., Horn, D., Kayserili, H., …
805 Mundlos, S. (2015). Disruptions of topological chromatin domains cause pathogenic rewiring of
806 gene-enhancer interactions. *Cell*, *161*(5), 1012–1025. https://doi.org/10.1016/j.cell.2015.04.004

807 Lyu, P., Hoang, T., Santiago, C. P., Thomas, E. D., Timms, A. E., Appel, H., Gimmen, M., Le, N., …
808 Blackshaw, S. (2021). Gene regulatory networks controlling temporal patterning, neurogenesis,
809 and cell-fate specification in mammalian retina. *Cell Reports*, *37*(7).
810 https://doi.org/10.1016/j.celrep.2021.109994

Marchal, C., Singh, N., Batz, Z., Advani, J., Jaeger, C., Corso-Díaz, X., & Swaroop, A. (2022). High-resolution genome topology of human retina uncovers super enhancer-promoter interactions at tissue-specific and multifactorial disease loci. *Nature Communications*, *13*(1), 1–16. https://doi.org/10.1038/s41467-022-33427-1

Martin, A. R., Williams, E., Foulger, R. E., Leigh, S., Daugherty, L. C., Niblock, O., Leong, I. U. S., Smith, K. R., … McDonagh, E. M. (2019). PanelApp crowdsources expert knowledge to establish consensus diagnostic gene panels. *Nature Genetics*, *51*(11), 1560–1565. https://doi.org/10.1038/s41588-019-0528-2

Martin, V., Zhao, J., Afek, A., Mielko, Z., & Gordân, R. (2019). QBiC-Pred: Quantitative predictions of transcription factor binding changes due to sequence variants. *Nucleic Acids Research*, *47*(W1), W127–W135. https://doi.org/10.1093/nar/gkz363

Martínez, F., Monfort, S., Rosellá, M., Oltra, S., Blesa, D., Quiroga, R., Mayo, S., & Orellana, C. (2010). Enrichment of ultraconserved elements among genomic imbalances causing mental delay and congenital anomalies. *BMC Medical Genomics*, *3*. https://doi.org/10.1186/1755-8794-3-54

McLean, C. Y., Bristor, D., Hiller, M., Clarke, S. L., Schaar, B. T., Lowe, C. B., Wenger, A. M., & Bejerano, G. (2010). GREAT improves functional interpretation of cis-regulatory regions. *Nature Biotechnology*, *28*(5), 495–501. https://doi.org/10.1038/nbt.1630

Morris, A. C., & Fadool, J. M. (2005). Studying rod photoreceptor development in zebrafish. *Physiology and Behavior*, *86*(3), 306–313. https://doi.org/10.1016/j.physbeh.2005.08.020

Pachano, T., Haro, E., & Rada-Iglesias, A. (2022). Enhancer-gene specificity in development and disease. *Development (Cambridge, England)*, *149*(11). https://doi.org/10.1242/dev.186536

Pedersen, H. R., Baraas, R. C., Landsend, E. C. S., Utheim, O. A., Utheim, T. P., Gilson, S. J., & Neitz, M. (2020). PAX6 genotypic and retinal phenotypic characterization in congenital aniridia. *Investigative Ophthalmology and Visual Science*, *61*(5). https://doi.org/10.1167/IOVS.61.5.14

Pennacchio, L. A., Ahituv, N., Moses, A. M., Prabhakar, S., Nobrega, M. A., Shoukry, M., Minovitsky, S., Dubchak, I., … Rubin, E. M. (2006). In vivo enhancer analysis of human conserved non-coding sequences. *Nature*, *444*(7118), 499–502. https://doi.org/10.1038/nature05295

Pituello, F., Medevielle, F., Foulquier, F., & Duprat, A. M. (1999). Activation of Pax6 depends on somitogenesis in the chick embryo cervical spinal cord. *Development*, *126*(3), 587–596. https://doi.org/10.1242/dev.126.3.587

Plaisancié, J., Tarilonte, M., Ramos, P., Jeanton-Scaramouche, C., Gaston, V., Dollfus, H., Aguilera, D., Kaplan, J., … Corton, M. (2018). Implication of non-coding PAX6 mutations in aniridia. *Human Genetics*, *137*(10), 831–846. https://doi.org/10.1007/s00439-018-1940-x

Polychronopoulos, D., King, J. W. D., Nash, A. J., Tan, G., & Lenhard, B. (2017). Conserved non-coding elements: Developmental gene regulation meets genome organization. *Nucleic Acids Research*, *45*(22), 12611–12624. https://doi.org/10.1093/nar/gkx1074

Quinlan, A. R., & Hall, I. M. (2010). BEDTools: A flexible suite of utilities for comparing genomic features. *Bioinformatics*, *26*(6), 841–842. https://doi.org/10.1093/bioinformatics/btq033

Rada-Iglesias, A., Bajpai, R., Swigut, T., Brugmann, S. A., Flynn, R. A., & Wysocka, J. (2011). A unique chromatin signature uncovers early developmental enhancers in humans. *Nature*, *470*(7333), 279–285. https://doi.org/10.1038/nature09692

Rapaport, D. H., Wong, L. L., Wood, E. D., Yasumura, D., & Lavail, M. M. (2004). Timing and topography of cell genesis in the rat retina. *Journal of Comparative Neurology*, *474*(2), 304–324.

https://doi.org/10.1002/cne.20134

Raychaudhuri, S., Iartchouk, O., Chin, K., Tan, P. L., Tai, A. K., Ripke, S., Gowrisankar, S., Vemuri, S., … Seddon, J. M. (2011). A rare penetrant mutation in CFH confers high risk of age-related macular degeneration. *Nature Genetics*, *43*(12), 1232–1236. https://doi.org/10.1038/ng.976

Rogers, M. F., Shihab, H. A., Mort, M., Cooper, D. N., Gaunt, T. R., & Campbell, C. (2018). FATHMM-XF: Accurate prediction of pathogenic point mutations via extended features. *Bioinformatics*, *34*(3), 511–513. https://doi.org/10.1093/bioinformatics/btx536

Santana-Garcia, W., Castro-Mondragon, J. A., Padilla-Gálvez, M., Nguyen, N. T. T., Elizondo-Salas, A., Ksouri, N., Gerbes, F., Thieffry, D., … Medina-Rivera, A. (2022). RSAT 2022: regulatory sequence analysis tools. *Nucleic Acids Research*, *50*(W1), W670–W676. https://doi.org/10.1093/nar/gkac312

Santos-Rosa, H., Schneider, R., Bannister, A. J., Sherriff, J., Bernstein, B. E., Emre, N. C. T., Schreiber, S. L., Mellor, J., & Kouzarides, T. (2002). Active genes are tri-methylated at K4 of histone H3. *Nature*, *419*(6905), 407–411. https://doi.org/10.1038/nature01080

Schmitt, E. A., & Dowling, J. E. (1999). Early retinal development in the Zebrafish, Danio rerio: Light and electron microscopic analyses. *Journal of Comparative Neurology*, *404*(4), 515–536. https://doi.org/10.1002/(SICI)1096-9861(19990222)404:4<515::AID-CNE8>3.0.CO;2-A

Schwarz, J. M., Hombach, D., Köhler, S., Cooper, D. N., Schuelke, M., & Seelow, D. (2019). RegulationSpotter: Annotation and interpretation of extratranscriptic DNA variants. *Nucleic Acids Research*, *47*(W1), W106–W113. https://doi.org/10.1093/nar/gkz327

Shi, F.-Y., Wang, Y., Huang, D., Liang, Y., Liang, N., Chen, X.-W., & Gao, G. (2021). Computational Assessment of the Expression-modulating Potential for Noncoding Variants. *Genomics, Proteomics & Bioinformatics*, *86*. https://doi.org/10.1016/j.gpb.2021.10.003

Small, K. W., DeLuca, A. P., Whitmore, S. S., Rosenberg, T., Silva-Garcia, R., Udar, N., Puech, B., Garcia, C. A., … Stone, E. M. (2016). North Carolina Macular Dystrophy Is Caused by Dysregulation of the Retinal Transcription Factor PRDM13. *Ophthalmology*, *123*(1), 9–18. https://doi.org/10.1016/j.ophtha.2015.10.006

Smedley, D., Smith, K. R., Martin, A., Thomas, E. A., McDonagh, E. M., Cipriani, V., Ellingford, J. M., Arno, G., … Caulfield, M. (2021). 100,000 Genomes Pilot on Rare-Disease Diagnosis in Health Care — Preliminary Report. *New England Journal of Medicine*, *385*(20), 1868–1880. https://doi.org/10.1056/nejmoa2035790

Snetkova, V., Pennacchio, L. A., Visel, A., & Dickel, D. E. (2021). Perfect and imperfect views of ultraconserved sequences. *Nature Reviews Genetics*, *0123456789*. https://doi.org/10.1038/s41576-021-00424-x

Snetkova, V., Ypsilanti, A. R., Akiyama, J. A., Mannion, B. J., Plajzer-Frick, I., Novak, C. S., Harrington, A. N., Pham, Q. T., … Dickel, D. E. (2021). Ultraconserved enhancer function does not require perfect sequence conservation. *Nature Genetics*, *53*(4), 521–528. https://doi.org/10.1038/s41588-021-00812-3

Soneson, C., Love, M. I., & Robinson, M. D. (2016). Differential analyses for RNA-seq: Transcript-level estimates improve gene-level inferences. *F1000Research*, *4*, 1–23. https://doi.org/10.12688/F1000RESEARCH.7563.2

Spielmann, M., & Mundlos, S. (2016). Looking beyond the genes: The role of non-coding variants in human disease. *Human Molecular Genetics*, *25*(R2), R157–R165. https://doi.org/10.1093/hmg/ddw205

898 Taylor, R. L., Poulter, J. A., Downes, S. M., McKibbin, M., Khan, K., Inglehearn, C. F., Webster, A. R.,
899 Hardcastle, A. J., … van Heyningen, V. (2019). Loss-of-Function Mutations in the CFH Gene
900 Affecting Alternatively Encoded Factor H-like 1 Protein Cause Dominant Early-Onset Macular
901 Drusen. *Ophthalmology*, *126*(10), 1410–1421. https://doi.org/10.1016/j.ophtha.2019.03.013

902 Thomas, E. D., Timms, A. E., Giles, S., Harkins-Perry, S., Lyu, P., Hoang, T., Qian, J., Jackson, V. E., …
903 Cherry, T. J. (2022). Cell-specific cis-regulatory elements and mechanisms of non-coding genetic
904 disease in human retina and retinal organoids. *Developmental Cell*, *57*(6), 820-836.e6.
905 https://doi.org/10.1016/j.devcel.2022.02.018

906 Thormann, A., Halachev, M., McLaren, W., Moore, D. J., Svinti, V., Campbell, A., Kerr, S. M.,
907 Tischkowitz, M., … FitzPatrick, D. R. (2019). Flexible and scalable diagnostic filtering of genomic
908 variants using G2P with Ensembl VEP. *Nature Communications*, *10*(1), 1–10.
909 https://doi.org/10.1038/s41467-019-10016-3

910 Turner, D. L., & Cepko, C. L. (1988). A common progenitor for neurons and glia persists in rat retina
911 late in development. *Nature*, *328*(6126), 131–136. https://doi.org/10.1038/328131a0

912 Turner, D. L., Snyder, E. Y., & Cepko, C. L. (1990). Lineage-independent determination of cell type in
913 the embryonic mouse retina. *Neuron*, *4*(6), 833–845. https://doi.org/10.1016/0896-
914 6273(90)90136-4

915 Van de Sompele, S., Small, K. W., Cicekdal, M. B., Soriano, V. L., D'haene, E., Shaya, F. S., Agemy, S.,
916 Van der Snickt, T., … De Baere, E. (2022). Multi-omics approach dissects cis-regulatory
917 mechanisms underlying North Carolina macular dystrophy, a retinal enhanceropathy. *American*
918 *Journal of Human Genetics*, *109*(11), 2029–2048. https://doi.org/10.1016/j.ajhg.2022.09.013

919 Visel, A., Minovitsky, S., Dubchak, I., & Pennacchio, L. A. (2007). VISTA Enhancer Browser - A database
920 of tissue-specific human enhancers. *Nucleic Acids Research*, *35*(SUPPL. 1), 88–92.
921 https://doi.org/10.1093/nar/gkl822

922 Vitsios, D., Dhindsa, R. S., Middleton, L., Gussow, A. B., & Petrovski, S. (2021). Prioritizing non-coding
923 regions based on human genomic constraint and sequence context with deep learning. *Nature*
924 *Communications*, *12*(1), 1–14. https://doi.org/10.1038/s41467-021-21790-4

925 Watanabe, S., Sanuki, R., Sugita, Y., Imai, W., Yamazaki, R., Kozuka, T., Ohsuga, M., & Furukawa, T.
926 (2015). Prdm13 regulates subtype specification of retinal amacrine interneurons and modulates
927 visual sensitivity. *Journal of Neuroscience*, *35*(20), 8004–8020.
928 https://doi.org/10.1523/JNEUROSCI.0089-15.2015

929 Whittaker, D. E., Oleari, R., Gregory, L. C., Le Quesne-Stabej, P., Williams, H. J., Torpiano, J. G.,
930 Formosa, N., Cachia, M. J., … Dattani, M. T. (2021). A recessive PRDM13 mutation results in
931 congenital hypogonadotropic hypogonadism and cerebellar hypoplasia. *Journal of Clinical*
932 *Investigation*, *131*(24). https://doi.org/10.1172/JCI141587

933 Wieczorek, D., Pawlik, B., Li, Y., Akarsu, N. A., Caliebe, A., May, K. J. W., Schweiger, B., Vargas, F. R., …
934 Wollnik, B. (2010). A specific mutation in the distant sonic hedgehog (SHH) cis-regulator (ZRS)
935 causes Werner Mesomelic Syndrome (WMS) while complete ZRS duplications underlie Haas
936 type polysyndactyly and preaxial polydactyly (PPD) with or without triphalangeal thumb.
937 *Human Mutation*, *31*(1), 81–89. https://doi.org/10.1002/humu.21142

938 Woolfe, A., Goode, D. K., Cooke, J., Callaway, H., Smith, S., Snell, P., McEwen, G. K., & Elgar, G. (2007).
939 CONDOR: A database resource of developmentally associated conserved non-coding elements.
940 *BMC Developmental Biology*, *7*, 1–11. https://doi.org/10.1186/1471-213X-7-100

941 Xie, Z., Bailey, A., Kuleshov, M. V., Clarke, D. J. B., Evangelista, J. E., Jenkins, S. L., Lachmann, A.,

942 Wojciechowicz, M. L., … Ma'ayan, A. (2021). Gene Set Knowledge Discovery with Enrichr.
943 *Current Protocols*, *1*(3), 1–51. https://doi.org/10.1002/cpz1.90

944 Yokoi, T., Nishina, S., Fukami, M., Ogata, T., Hosono, K., Hotta, Y., & Azuma, N. (2016). Genotype–
945 phenotype correlation of PAX6 gene mutations in aniridia. *Human Genome Variation*, *3*(1), 1–5.
946 https://doi.org/10.1038/HGV.2015.52

947 Zhang, X., Leavey, P., Appel, H., Makrides, N., & Blackshaw, S. (2023). Molecular mechanisms
948 controlling vertebrate retinal patterning, neurogenesis, and cell fate specification. *Trends in*
949 *Genetics : TIG*, 1–22. https://doi.org/10.1016/j.tig.2023.06.002

950 Zhang, Y., Liu, T., Meyer, C. A., Eeckhoute, J., Johnson, D. S., Bernstein, B. E., Nussbaum, C., Myers, R.
951 M., … Shirley, X. S. (2008). Model-based analysis of ChIP-Seq (MACS). *Genome Biology*, *9*(9).
952 https://doi.org/10.1186/gb-2008-9-9-r137

953 Zhou, J., & Troyanskaya, O. G. (2015). Predicting effects of noncoding variants with deep learning-
954 based sequence model. *Nature Methods*, *12*(10), 931–934.
955 https://doi.org/10.1038/nmeth.3547

956

SUPPLEMENTARY MATERIAL

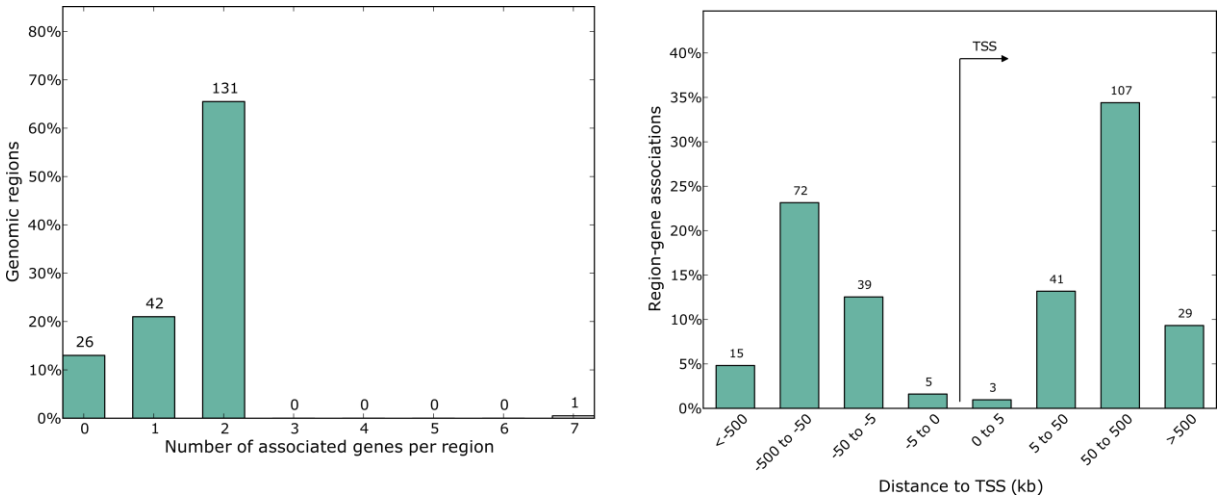

Figure S1. Distribution of target genes associated with random genomic background. To evaluate potential confounding effects of the random genomic background, *GREAT* was used to assign their corresponding target genes. No significant differences were observed in distribution of the number of associated genes (*right*) or distances from transcription start sites (*left*) compared to those of the UCNEs (Fig. 2A-B).

A

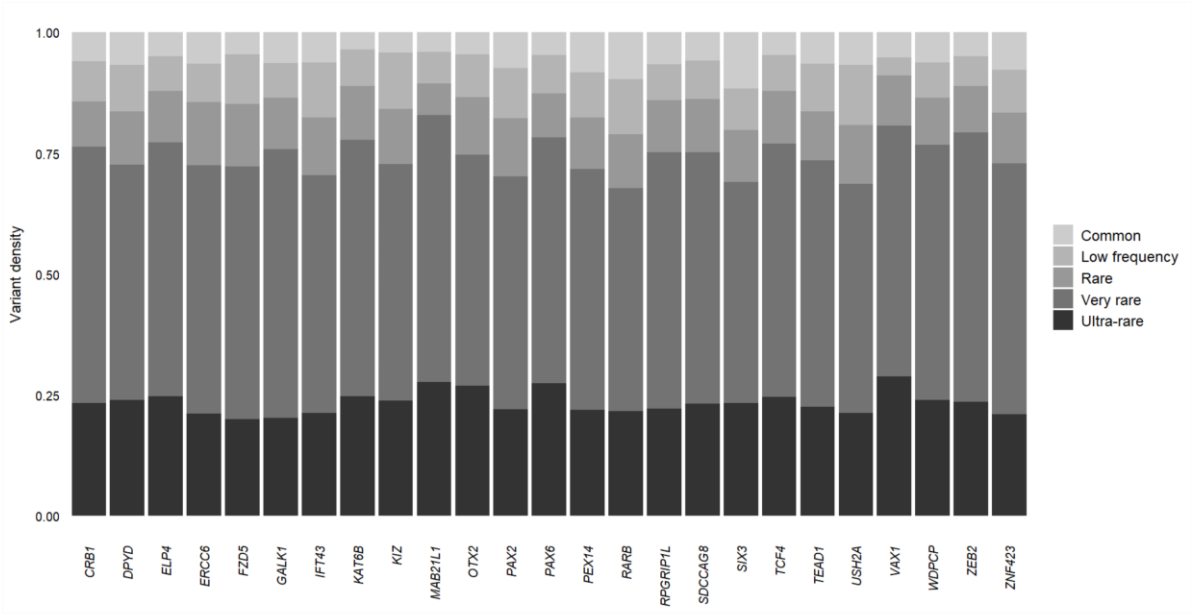

B

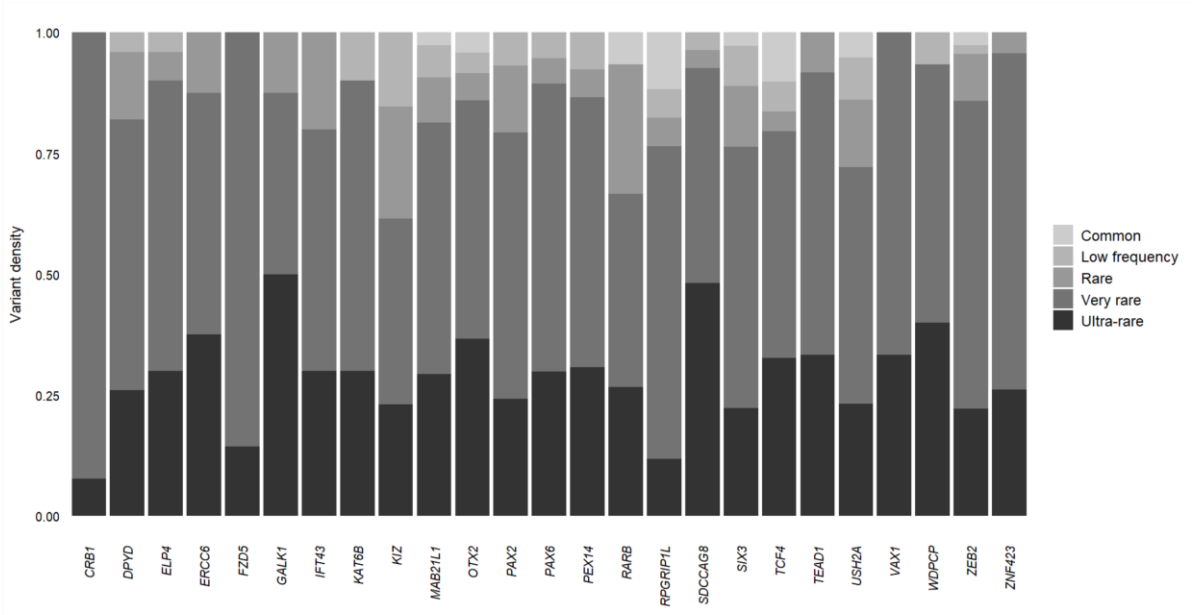

Figure S2. Allele frequency distribution of disease-associated genes and their respective UCNEs. For a selection of 25 disease-associated genes (**A**) and their corresponding UCNEs (**B**), allele frequency distributions were generated to assess the specificity of the overlap between rare variants and UCNEs.

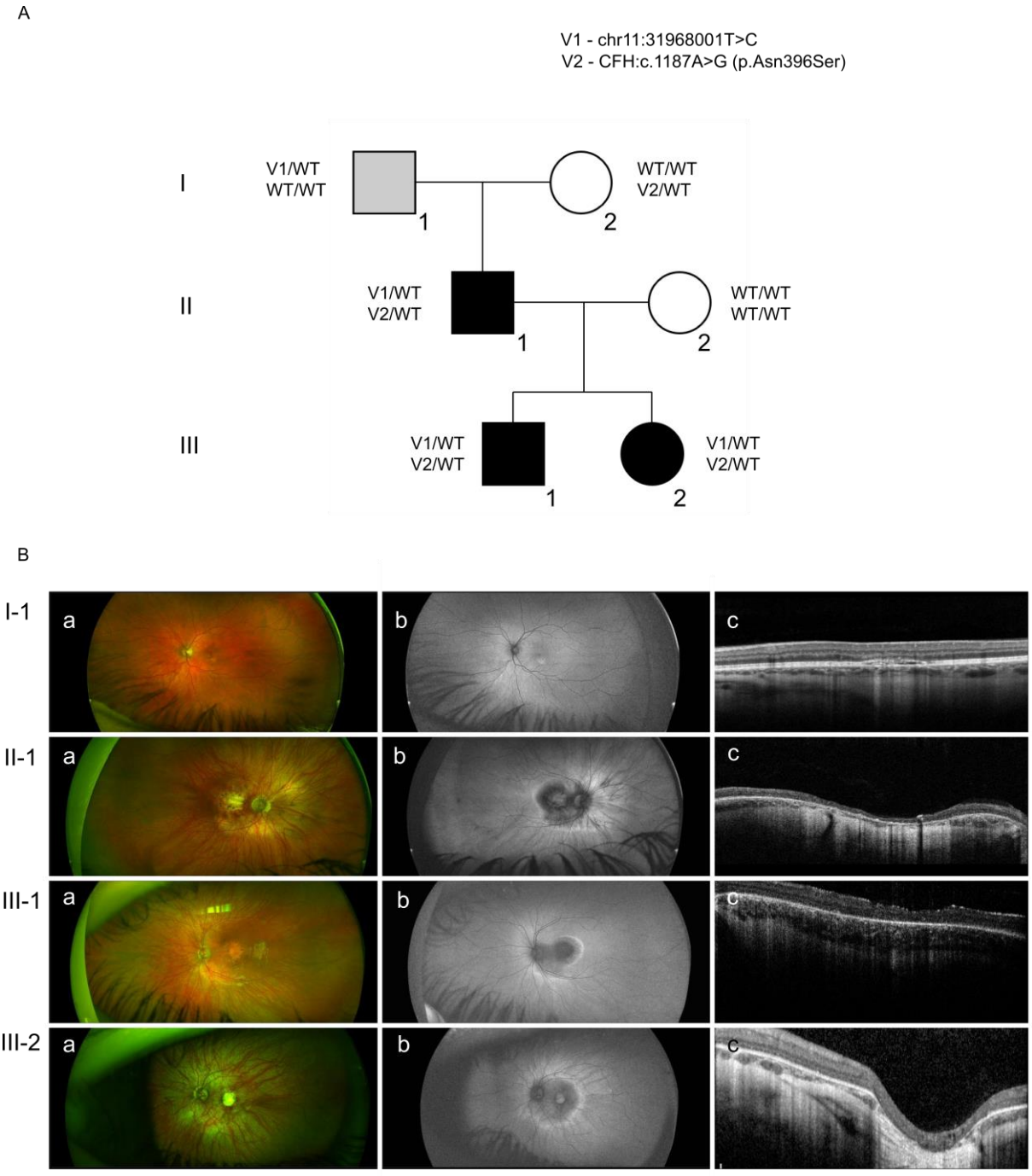

Figure S3. *PAX6*-associated variant exclusively found in a family presenting foveal anomalies. A) Pedigree of the family, indicating segregation of the *PAX6*-associated UCNE variant (V1) and of the *CFH* variant (V2). **B)** Ophthalmological assessment (fundus examination, FAF, and OCT) revealed tessellated fundi with atrophic areas at the macula involving the fovea in II-1, III-1 and III-2, while I-1 displayed only an area of pallor inferior to the left fovea and corresponding hyper-autofluorescence (see Table S7).

A

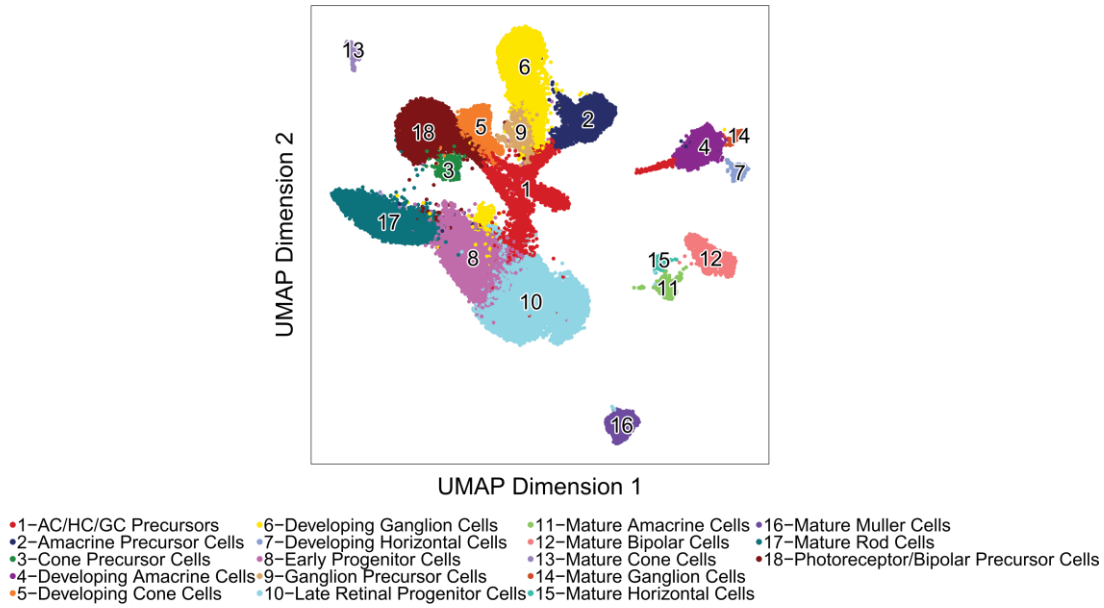

B

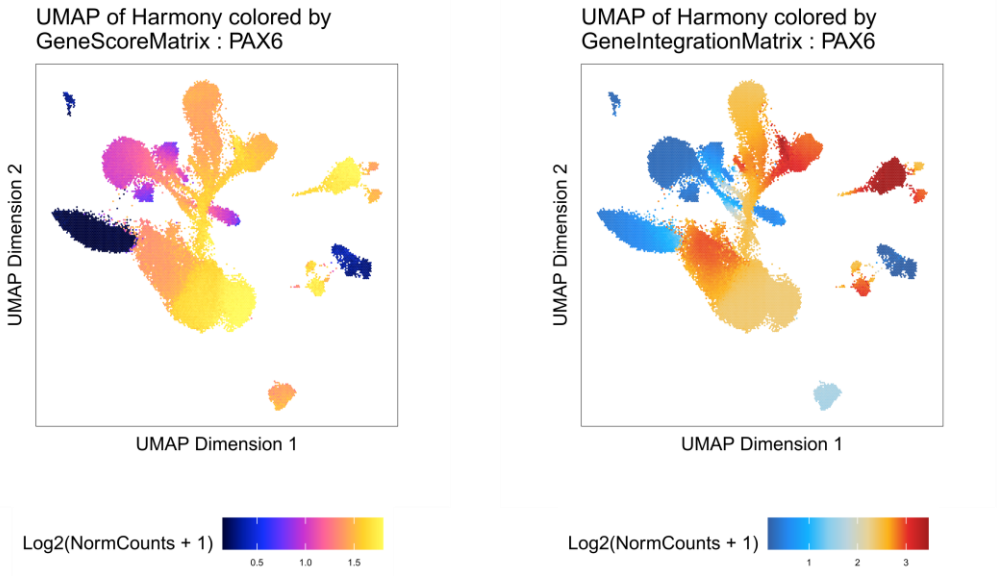

Figure S4. Single-cell characterization of the *PAX6* gene. A) UMAP of the analyzed single cell dataset (Thomas et al., 2022).**B)** Feature plots (scATAC-seq and scRNA-seq) for the *PAX6* locus.

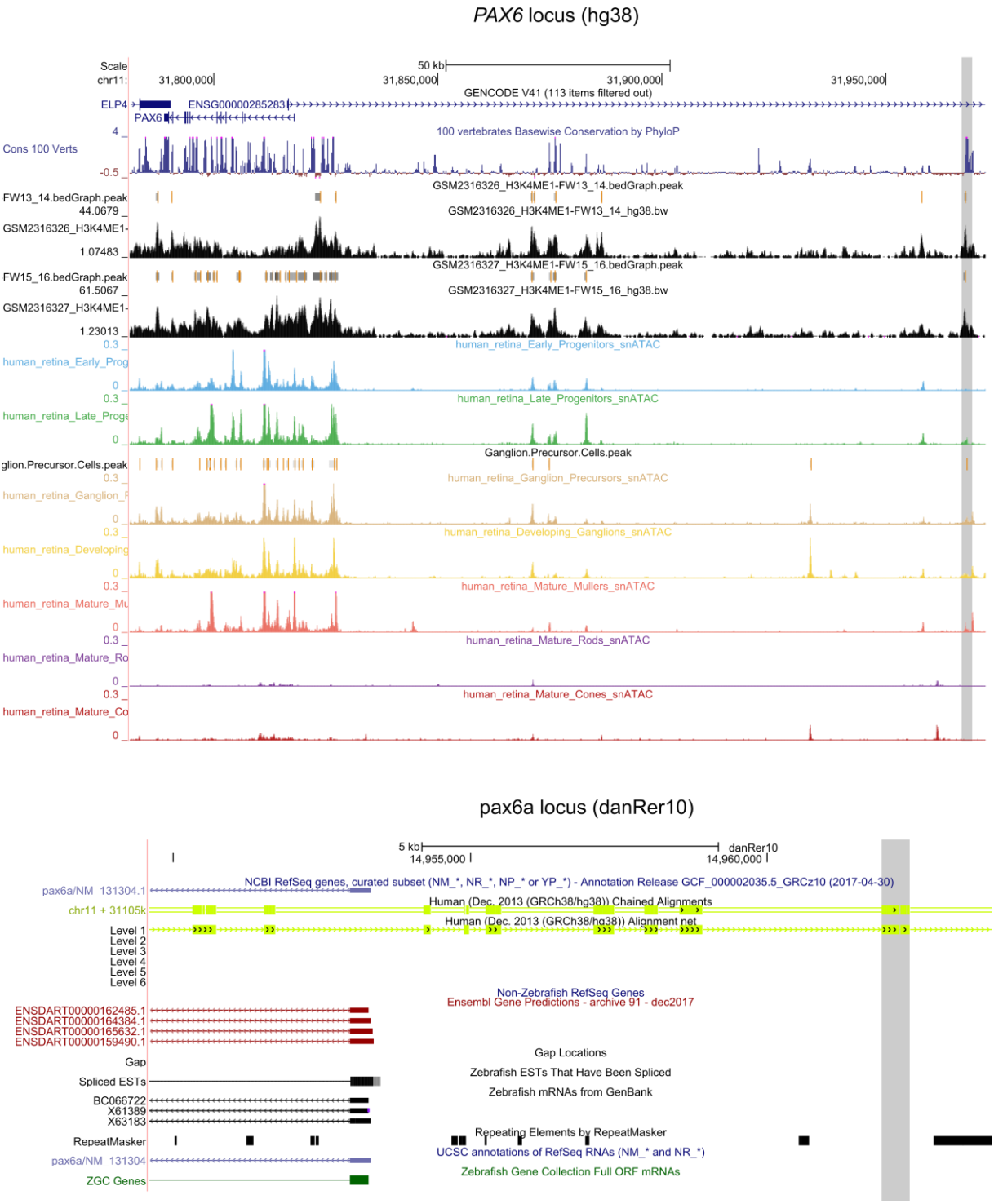

Figure S5. Syntenic region in zebrafish of the human *PAX6* locus. Location of the characterized UCNE (*in gray*, *PAX6_Veronica*) linked to *PAX6*, found exclusively in the *pax6a* locus of zebrafish at a shorter distance (≈15kb) when compared to the human *PAX6* locus (≈150kb) with respect to the *PAX6* transcription start site.

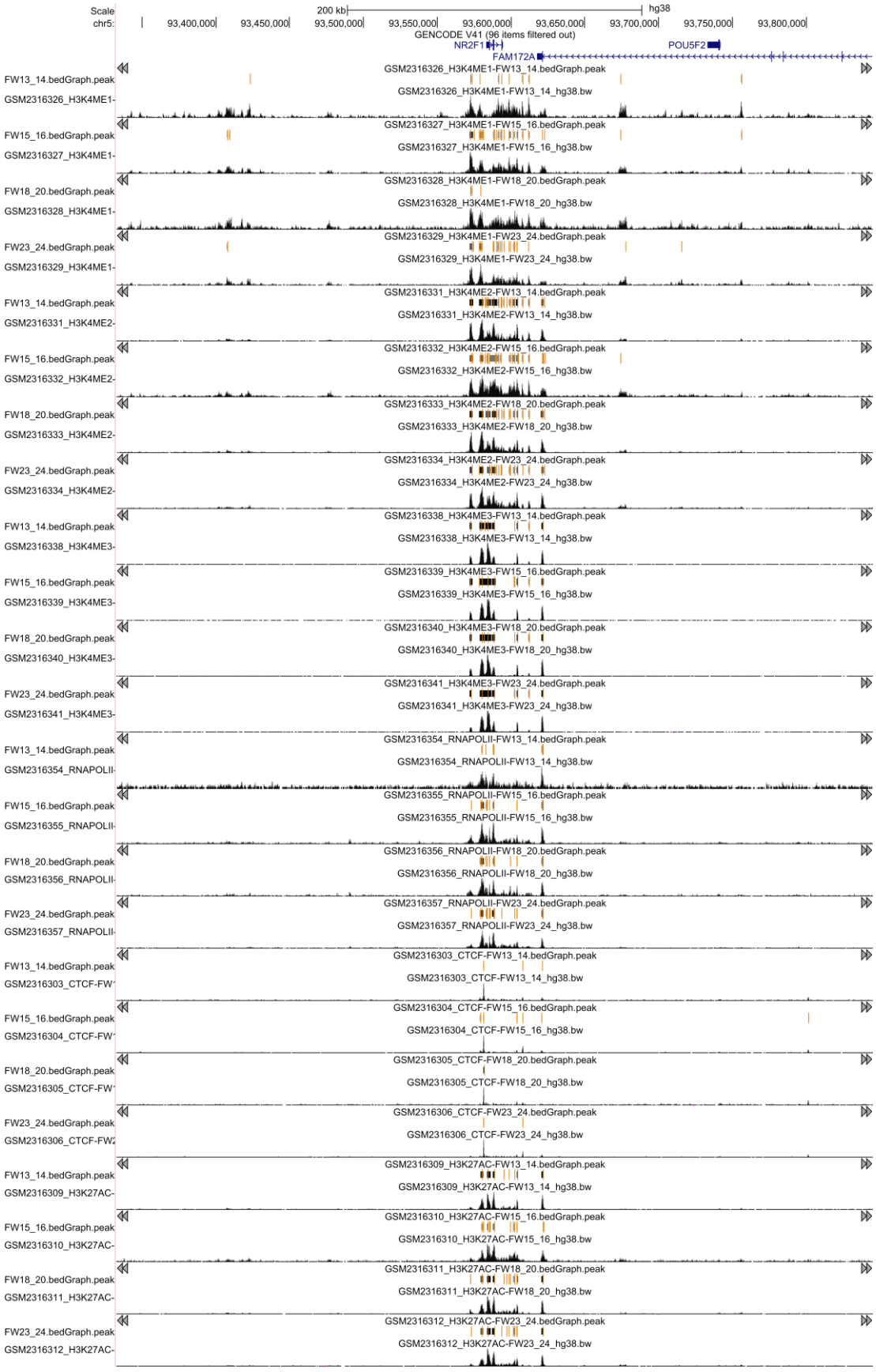

Figure S6. Peak identification of scATAC-seq and ChIP-seq data. A) Peak identification within the *NR2F1* locus for the following marks: H3K4me1, H3K4me2, H3K4me3, CTCF, RNAPolII and H3K27ac across the different time points.

Table S1. Characterization of UCNEs based on: UCNE ID – Original UCNE unique identifier from (Dimitrieva et al., 2013); **g.coordinates (hg38) –** genomic coordinate of the UCNE; **Type –** original classification of UCNE (Dimitrieva et al., 2013) based on the genomic location of UCNE with respect to its overlapping gene; **Distance to TSS of target gene –** genomic distance between UCNE and the transcription start site of its target gene (bp); **Target gene –** gene association extracted from GREAT analysis; **Bulk RNA-seq (target gene mean expression) –** expression value (TPM) obtained from the RNA-seq based on samples related to the human retinal development (Hoshino et al., 2018); **Bulk RNA-seq (target gene expression rank) –** expression rank obtained from the RNA-seq based on samples related to the human retinal development from (Hoshino et al., 2018); **Bulk RNA-seq (target gene maximum expression) –** maximum values of gene expression (TPM) obtained from the RNA-seq based on samples related to the human retinal development (Hoshino et al., 2018); **Bulk RNA-seq (stage of maximum target gene expression)** – stage where the maximum levels of gene expression where observed, obtained from the RNA-seq based on samples related to the human retinal development (Hoshino et al., 2018); **scRNA-seq target gene expression –** retinal cell cluster where the expression of the target gene is expected, obtained from the scRNA-seq based on samples related to human retinas (Thomas et al., 2022); **DNase-seq (stage)** – stages where the open chromatin context was identified, obtained from the DNase-seq experiments related to the retinal development (ENCODE); **scATAC-seq** – cell clusters where the peak identification was retrieved (Thomas et al. 2022); **Retinal TAD Support** – qualitative estimation of the association UCNE-target gene; **ChIP-seq** - epigenomic marks, CTCFs and PolII peaks observed within the genomic context of the characterized UCNE (Aldiri et al. 2017 , Cherry et al. 2020); **VISTA (Element ID)** – assessment of the inclusion of the UCNE element within the VISTA enhancer browser and its unique ID; **VISTA (Assay result)** – reporter assay result from the VISTA enhancer browser; **VISTA (Expression pattern) –** includes the tissues where the expression pattern for the reporter assay was observed.

Table S2. Characterization of UCNEs based on epigenomic marks.

Table S3. Full gene set ontology enrichment results from *Enrichr*.

Table S4. Comparison between target genes assigned by *GREAT* and peak-to-gene linkage method.

Table S5. Disease association of UCNE target genes. #OMIM disease name; confidence category; allelic requirement; mutation consequence; phenotypes; organ specificity list; PMIDs. Additional genomic and functional annotations are the same as in Table S1.

Table S6. Overview of the eye disease sub-cohort of 100,000 Genomes Project (Genomics England). Normalized Disease Group, sub group, and specific disease; Participant Count.

Table S7. Variants retrieved within the UCNEs that are linked to an eye or retinal disease phenotype. It includes the **gene**, the **UCNE ID** and its **coordinates,** and the retrieved **variant** (hg38).

Table S8. Phenotypic description of the studied family segregating autosomal dominant foveal abnormalities. P**articipant information** (ID, origin and sex), **molecular findings** (carriers of the V1 (chr11:31968001T>C) and/or V2 (CFH, c.1187A>G (p.Asn396Ser)), **diagnosis** and **age of onset** (Clinical diagnosis, Age at diagnosis, Age of onset visual field loss, Age of onset BCVA loss) and **clinical findings.**

Table S9. Analysis of the TFBS motif disruption potentially exerted by the chr11:31968001T>C variant (qBiC-PRED) and retrieved variants within genes associated with macular developmental defects and foveal hypoplasia (*IRX1*, *PRMD13*, *SLC38A8*, *GPR143*, *FRMD7* and *AHR*). Output from qBiC-PRED includes the predicted TF binding changes, associated name in protein binding microarray experiments (pbmname), the normalized changes (z-scores), the significance of the changes according to each model (p.value), and the predicted changes in binding status (e.g. bound > unbound).

Table S10. Overview of the transgenic enhancer assays in zebrafish for the *PAX6*-associated UCNE.

Table S11. Overview of the datasets used in this study.

Table S12. Set of primers used in this study for cloning and segregation.